Predicting solvent degradation in absorption–based CO_2 capture from industrial flue gases

Lucas Braakhuis, Hanna K. Knuutila [*]

Department of Chemical Engineering, Norwegian University of Science and Technology (NTNU), NO-7491 Trondheim, Norway

ARTICLE INFO

ABSTRACT

This work aims to predict solvent degradation rates in absorption-based CO_2 capture processes using a 30 wt% aqueous monoethanolamine (MEA) solvent. A degradation model for MEA is developed and used to predict solvent degradation in full-scale capture processes. Mass transfer resistances and the solubility of O_2 are considered to obtain a generalized and consistent degradation model. Degradation is evaluated for the capture process for flue gases with typical industrial compositions; a natural gas-fired power plant, a waste-to-energy plant, a coal-fired– power plant, and a cement plant. The impact of process modifications, such as absorber intercooling, dissolved O_2 removal, a reduction in solvent residence times, and increased stripper pressures on degradation is evaluated.

The predicted degradation rate in the capture processes is approximately 90 to 150 g MEA/ton CO_2 captured, and the composition of the flue gas was found to have a significant influence on the distribution of degradation throughout the process. Modifications to the process can significantly affect the overall degradation rate. Both absorber intercooling and removal of dissolved O_2 may reduce the overall degradation by up to 40%, depending on the composition of the flue gas. A reduction in solvent residence times or pressure in the stripper has limited effects on the degradation in the case of MEA, because of the amine's relatively low stability towards oxidative degradation. However, these process modifications look promising for more stable solvents.

1. Introduction

Carbon capture processes using amine-based absorbents can play an essential role in reducing carbon emissions from industrial plants, not only in the short term but also in the future in case of hard-to-abate industries, such as waste-to-energy and the production of metals, cement, and silicon (Rogelj et al., 2018).

A good absorbent for CO_2 capture is not only characterized by favorable capture properties, such as fast kinetics, a high capacity, a low viscosity, and a low regeneration energy requirement but also by good stability and resistance towards degradation. (Reynolds et al., 2016) Solvent degradation results in the formation of degradation products and can reduce the solvent's capture capacity. These degradation compounds cause various operational issues, such as reduced capture performance, increased emissions, corrosion of equipment, and additional degradation. (Kohl and Nielsen, 1997; Martin et al., 2012; Vega et al., 2014) Therefore, it is crucial to consider degradation and possible mitigation and solvent treatment technologies, when designing a capture plant and developing operational strategies. Aside from a good

understanding of the degradation mechanisms, solvent degradation models that can predict degradation and product formation rates are important for developing these strategies.

Although several solvents have received more interest in recent years, monoethanolamine (MEA) is still one of the most researched solvents on both a laboratory and industrial scale. (Gouedard et al., 2012) Significant information is available on the physical and chemical properties of the solvent, the solubility of O_2, and degradation both in lab-scale reactors (Gouedard et al., 2012; Fredriksen and Jens, 2013) and industrial capture pilots and plants (Buvik et al., 2021). For these reasons, this work will primarily focus on MEA. However, the conclusions of this work may also apply to other solvents or solvent blends.

The most prominent solvent degradation mechanisms are oxidative and thermal degradation. Oxidative degradation is caused by the presence of O_2 in flue gas and thermal degradation occurs at increased temperatures. Various works in the literature have studied these types of degradation for MEA solvents. Thermal degradation is often studied by exposing the loaded solvent to high temperatures in closed batch reactors (Eide-Haugmo, 2011; Davis, 2009; Grimstvedt et al., 2013; Léonard et al., 2014), whereas oxidative degradation is typically studied

Nomenclature

Variable	Definition (Unit)
a_I	Interfacial area of bubbles (m^2/m^3)
$c_{i,L}$	Liquid (bulk) concentration of species i (mol/m_L^3)
$c_{i,I}$	Liquid interface concentration of species i (mol/m_L^3)
c_{i,H_2O}	Concentration of species i in water (mol/m_L^3)
D_i	Diffusion coefficient of species i (m^2/s)
d_b	Bubble diameter (m)
E_A	Activation energy J/mol
h_i	Ion specific parameter of species i ($m^3 \cdot kmol^{-1}$)
$h_{G,i}$	Gas-specific parameter of species i ($m^2 \cdot kmol^{-1}$)
$h_{T,i}$	Temperature dependence of the gas-specific parameter of species i ($m^3 \cdot kmol^{-1} K^{-1}$)

Variable	Definition (Unit)
J_i	Mass transfer flux of species i ($mol\ m^{-2} \cdot s^{-1}$)
k_L	Mass transfer coefficient (m/s)
k_r	Reaction rate coefficient (-)
k_{ref}	Reaction rate coefficient at T_{ref} (-)
P/V	Stirring power per volume (W/m^3)
p_{O_2}	Partial pressure of O_2 (atm)
R_i	Reaction rate ($mol \cdot m_L^{-3} \cdot s^{-1}$)
R_{id}	Ideal gas constant ($=8.314$) ($J \cdot K^{-1} \cdot mol^{-1}$)
T_{ref}	Reference temperature (K)
V_R	Reactor volume (m^3)
V_L	Liquid volume (m_L^3)
ϵ_L	Liquid volume fraction (m_L^3/m^3)
ρ_L	Density of the liquid (kg/m^3)
ν_L	Kinematic viscosity of the liquid (m^2/s)

in open or semi-open systems where O_2 is added to compensate for the O_2 consumed during the degradation (Léonard et al., 2014; Supap et al., 2001; Vevelstad et al., 2016; Lepaumier et al., 2009; Goff and Rochelle, 2004). In some cases, degradation models have been developed based on the results from the lab scale degradation experiments (Davis, 2009; Léonard et al., 2014; Braakhuis and Knuutila, 2021; Supap et al., 2009; Uyanga and Idem, 2007).

Some of these kinetic models have been used to evaluate solvent degradation in a full–scale capture process, such as in the works by Léonard et al. (Léonard et al., 2015) and Dhingra et al. (Dhingra et al., 2017). However, the assumptions and decisions that were made when developing the kinetic model using the lab–scale experiments are not always valid or logical with respect to the full–scale process. This includes neglecting mass transfer resistances in the experiments or the inconsistent use of O_2 solubility models. Therefore, the predictions made for the full-scale process are likely inaccurate.

This work aims to develop a degradation model for MEA and use it to predict solvent degradation in full-scale capture processes. The degradation model is developed such that it is consistent and applicable for both lab-scale experiments and full-scale plants. Degradation is evaluated for the capture process for flue gases with typical industrial compositions; a natural gas-fired power plant, a waste-to-energy plant, a coal–fired power plant, and a cement plant. The impact of process modifications, such as absorber intercooling, dissolved O_2 removal, a reduction in solvent residence times, and increased stripper pressures on degradation is evaluated. The degradation model is connected Aspen Plus, where steady-state process simulations were performed to get process data for the degradation model.

The degradation model presented here will primarily focus on the solvent loss through degradation and not on the type and quantity of the formed degradation products. The degradation model is limited to thermal and oxidative degradation as these degradation mechanisms are responsible for the majority of solvent degradation in most capture processes (Veltman et al., 2010). Thermal degradation is described using a previously developed model (Braakhuis and Knuutila, 2021), whereas a new oxidative degradation model is constructed in this work. This oxidative model takes into account the mechanisms for solubility and mass transfer of O_2 for oxidative degradation and is therefore applicable to both the degradation experiments and the full-scale processes.

The lack of experimental data on the corrosion of stainless steels in the presence of degradation products, along with the solubility of corroded metals and their influence on degradation rate, makes it difficult to accurately model these effects. Therefore, this study does not address accelerated degradation as a result of these factors (Goff, 2005; Léonard et al., 2014; Chi, 2000). Although the predictions in this work may not always fully correspond with observations in real–life processes, the work still offers needed insights into the extent and distribution of degradation and the effect of mitigation strategies.

1.1. Oxidative degradation modeling

Oxidative degradation is a complex process that involves both the transfer of O_2 from the gas to the liquid phase and a sequential liquid phase reaction of the dissolved O_2 with the amine. The observed amine degradation rate is thus a function of O_2 solubility, mass transfer resistances, and kinetic reaction parameters (Vega et al., 2014; Goff and Rochelle, 2004). Relevant process parameters, such as temperature, O_2 partial pressure, MEA concentration, and CO_2 loading, influence each of these mechanisms. It can be challenging to isolate, quantify, and model these mechanisms individually. As a result, models developed using specific experimental setups may be inaccurate when evaluating degradation in industrial equipment with a different geometry.

In a typical capture plant, oxidative degradation can be classified into two types: direct and indirect oxidative degradation. Direct oxidative degradation occurs when the solvent is in direct contact with the flue gas. The dissolved O_2 in the solvent can be replenished to some degree with O_2 from the flue gas as the degradation reactions consume it. This type of oxidative degradation occurs, for example, in the absorber packing. Indirect oxidative degradation, on the other hand, occurs when there is no direct contact with the flue gas but due to the presence of dissolved O_2. This type of degradation occurs in the piping and heat exchanger when the rich solvent is transported from the absorber to the stripper. The increased temperatures in some of these equipment may accelerate the degradation, up until the point at which all the dissolved O_2 is consumed.

A kinetic model for the oxidative degradation of MEA was developed by Uyanga et al. (Uyanga and Idem, 2007) and Supap et al. (Supap et al., 2009) using experiments in a semi-batch autoclave reactor. The temperatures of the experiments range from 100 °C to 120 °C, which is higher than those typically found in the absorber. Degradation in the presence of SO_2 was also investigated. However, this kinetic model doesn't distinguish between degradation through O_2, SO_2, or thermal degradation with CO_2, and only considers the total consumption of MEA. Further, the concentration of dissolved O_2 was assumed to be in equilibrium and was calculated using the correlation by Rooney et al. (Rooney and Daniels, 1998). This correlation does not consider the effect of CO_2 loading on the solubility of O_2.

Léonard et al. (Léonard et al., 2014; Léonard, 2013) also studied oxidative degradation of MEA and developed a kinetic model. Aside from a single experiment at 55 °C, the experiments were run at temperatures above 100 °C. The experiments were performed in a degradation reactor similar to the one used by Supap et al. (Supap et al., 2009), but a gas entrainment impeller was used to enhance the contact between the gas and liquid phases. Léonard (Léonard, 2013) showed a

linear relationship between the agitation rate and degradation experiments in their experimental work, indicating that mass transfer resistances play an important role in this type of degradation experiments. In a similar setup, Goff et al. (Goff and Rochelle, 2004) also observed increased degradation rates at higher agitation speeds.

In the kinetic model, Léonard et al. (Léonard et al., 2014) used Henry's law for O_2 in water to determine the concentration of O_2. Mass transfer limitations and the impact of the CO_2 loading on the solubility of O_2 were not considered, and the regressed kinetic constants may thus be underestimated. In the following work on predicting degradation in a capture process by Léonard et al. (Léonard et al., 2014), Henry's constant was also used to predict the concentration of O_2 in the solvent. Although this is consistent with the experimental modeling, the mass transfer mechanisms in the degradation experiments are different from those in the absorber, which could lead to inaccuracies in the results.

Additional modeling of solvent degradation in absorption-based capture processes was done by Dhingra et al. (Dhingra et al., 2017), where the extent of degradation in pilot plants was investigated and modeled. The oxidative reaction kinetics by Léonard et al. (Léonard et al., 2014) were used in combination with an O_2 solubility model that was fitted using experimental data by Wang et al. (Wang et al., 2013). This data, however, contains measurements of the O_2 solubility in loaded aqueous solutions of MEA and are thus not consistent with the used degradation model. Furthermore, the relatively high residence times in the pilot plants allow for flexibility in operation but are not representative of full-scale capture plants.

Oxidative degradation was studied at lower temperatures by Vevelstad et al. (Vevelstad et al., 2016), with experiments ranging from 55 °C to 75 °C. The experimental setup is similar to the one used by Léonard et al. (Léonard et al., 2014) but featured a gas recycle that allowed a higher gas flow rate and increased contact between the gas and liquid phase. Aside from the consumption of MEA, the formation of a broad set of degradation products was measured and quantified.

Pinto et al. (Pinto et al., 2014) used the experimental data by Vevelstad et al. (Vevelstad et al., 2016) to develop a multicomponent kinetic model, including the formation of degradation products. The complexity of oxidative degradation makes it challenging to describe the reaction pathways and identify the role of each of the components in the reaction rate equations. Assumptions regarding the reaction mechanisms had to be made by Pinto et al. (Pinto et al., 2014) and these are likely to have caused the observed uncertainties in the predictions of the model, especially for the degradation products. The predictions for MEA consumption were more accurate. However, the correlation by Rooney et al. (Rooney and Daniels, 1998) was also used in this work to calculate the solubility of O_2, thus not taking into account the effect of CO_2.

The CO_2 loading of the solvent plays a key role in the degradation experiments as it is found to decrease the oxidative degradation rate in several experimental works. Léonard (Léonard, 2013) observed a significant inhibiting effect of CO_2 loading compared to an unloaded solvent, but the degree of CO_2 loading appeared to have no effect. Supap et al. (Supap et al., 2009) and Kasikamphaiboon et al. (Kasikamphaiboon et al., 2015) observed a similar inhibiting effect in the autoclave experiments, but the authors did observe increased inhibition at higher CO_2 loadings. The decrease in degradation may be the effect of a reduced O_2 solubility since the presence of CO_2 in the solvent has been found to lower the O_2 solubility (Wang et al., 2013; Buvik et al., 2021).

The CO_2 can also increase the viscosity of the solvent, thereby reducing the diffusivity and mass transfer coefficient of O2 (Weiland et al., 1998). In case oxidative degradation is limited by mass transfer, a reduction in degradation is observed. The differences between the observations on the role of CO_2 may be explained by the different experimental reactor designs and their associated mass transfer resistances.

2. Methodology

2.1. Degradation framework

Solvent degradation is a gradual process that has little to no direct impact on the capture plant. It is the accumulation of degradation products and solvent consumption over time that changes the properties and performance of the solvent. It is, therefore, not necessary to implement a dynamic model that describes both kinetics of absorption/desorption and solvent degradation rates, but instead, a pseudo-steady state model can be used.

In the pseudo-steady state model, process conditions of the steady state simulation that are used to evaluate solvent degradation are assumed to be constant for a specific period of time. Changes in solvent composition as a result of degradation in this period are calculated, after which the solvent in the simulation is updated and the simulation is run again to obtain a new steady state. These steps are repeated for the duration of the entire modeled operational period. The time step size is chosen such that the difference in process conditions of consecutive simulations does not lead to significant changes in the degradation reaction rates.

An overview of the degradation framework that is used in this work is given in Fig. 1. The heart of the framework is the *Controller* module, which controls communication between all the other modules. The module opens a simulation and constructs an interface to communicate with the simulation software. From here, simulation parameters can be changed, the simulation can be executed, and simulation results can be retrieved.

The controller module uses the simulation results to construct a *Plant* object, which is a simplified model of the simulation that contains general information on the quality of the solvent as well as a set of *Equipment* objects. Each of the *Equipment* objects stores the simulation results of the corresponding equipment, so these can be used to evaluate the O_2 solubility or degradation models. For example, the *Equipment* object for a column stores process information (e.g., temperatures, partial pressures, liquid concentrations, and volumes) for various parts of the column, such as the packing, condenser, reboiler, or sump.

The *Controller* module uses the stored process information in each of the *Equipment* objects to evaluate the O_2 solubility and degradation models and calculate the predicted solvent consumption and degradation product formation for that *Equipment* object. These results are then stored in the objects themselves and combined to determine the overall degradation in the plant. The composition of the solvent in the process simulation can then be updated to evaluate the impact of the degradation on the capture process.

The modular structure of the framework allows for good customizability since new degradation modules or modules for other solvents can seamlessly replace the current ones. Additionally, new modules can be added seamlessly. Future extension modules could contain models on viscosity, corrosion, entrainment and evaporation, or reclaiming of the solvent.

2.2. Thermal degradation of MEA

Thermal degradation of the aqueous MEA solvent is described using a degradation model from one of our previous works (Braakhuis and Knuutila, 2021). The model was designed and fitted using experimental data on the concentrations of MEA and its degradation products when exposed to increased temperatures in closed cylinders. The data were collected from several independent works and contained results for aqueous solutions with 30 wt% of MEA at loadings between 0.1 and 0.5 mol CO_2/mol MEA and temperatures from 100 to 160 °C. The proposed degradation reactions, rate equations, and corresponding kinetic parameters for the model are given in Table 1. The reaction rate coefficient (k_r) is described using an alternative notation of the Arrhenius equation in Eq. *(1)*, which was used to simplify the fitting of the model
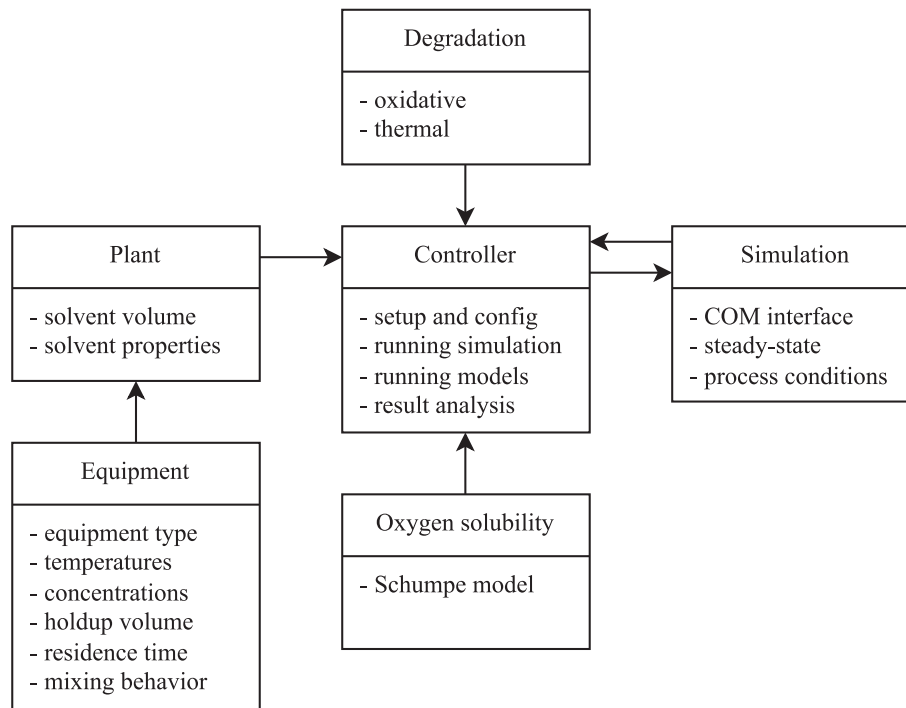
Fig. 1. Overview of the degradation framework and the corresponding modules.

Table 1

Proposed degradation reactions, reaction rate equations, and kinetic parameters for the thermal degradation model. (Braakhuis and Knuutila, 2021) The reference temperature (T_{ref}) is 400 K.

No.	Reaction	Reaction rate [mol·m^{-3}·s^{-1}]	k_{ref} [m^3·mol^{-1}·s^{-1}]	E_A [J/mol]
1	$2\,MEA \rightarrow HEEDA + H_2O$	$R_1 = k_{r,1}[MEA][CO_2]$	$1.599 \cdot 10^{-11}$	$1.511 \cdot 10^5$
2	$MEA + HEEDA \rightarrow TRIMEA$	$R_2 = k_{r,2}[HEEDA][CO_2]$	$1.117 \cdot 10^{-10}$	$1.215 \cdot 10^5$
3	$HEEDA + CO_2 \rightarrow HEIA$	$R_3 = k_{r,3}[HEEDA][CO_2]$	$3.054 \cdot 10^{-10}$	$1.426 \cdot 10^5$
4	$TRIMEA + CO_2 \rightarrow AEHEIA$	$R_4 = k_{r,4}[TRIMEA][CO_2]$	$2.839 \cdot 10^{-10}$	$1.362 \cdot 10^5$
5	$2\,MEA \rightarrow BHEU + H_2O$	$R_5 = k_{r,5}[MEA][CO_2]$	$5.170 \cdot 10^{-13}$	$1.511 \cdot 10^5$

parameters. The reference temperature (T_{ref}) for the coefficients is 400 K.

The activation energy for reaction no. 5 for the formation of 1,3-Bis (2-hydroxyethyl)urea (BHEU) could not be determined due to insufficient data for this compound at different temperatures. It is, however, expected to be comparable to the activation energy of reaction no. 1, because the reaction mechanisms are similar. (Braakhuis and Knuutila, 2021) Therefore, in this work, the same activation energy is used for reaction no. 5. Regardless of the temperature, the contribution of this reaction to the consumption of MEA is limited because the reaction rate coefficient is nearly two orders of magnitude smaller. The model can be safely extrapolated for temperatures below 100 °C since the predicted reaction rates are insignificant at these conditions.

$$k_r = k_{ref} \cdot \exp\left(\frac{-E_A}{R_{id}}\left(\frac{1}{T} - \frac{1}{T_{ref}}\right)\right) \tag{1}$$

2.3. Oxidative degradation of MEA

2.3.1. Oxygen solubility

The concentration of dissolved O_2 in the solvent is predicted using the gas solubility model for electrolyte solution by Schumpe et al. (Weisenberger and Schumpe, 1996), see Eq. (2) and Eq. (3). This model considers the effects of temperature and the concentration of ionic species in the solvent. Reduced O_2 solubility due to carbamate and carbonate species from CO_2 absorption can thus be modeled. The ion-specific model parameters for a loaded aqueous MEA solvent are taken

from the work by Buvik et al. (Buvik et al., 2021). The authors determined the ion–specific parameters for protonated MEA and the MEA carbamate using experimental data for the solubility of N_2O. In addition, the authors validated the model using experimental data and concluded that the modeling results were realistic (Buvik et al., 2021).

The parameters for the solubility model are given in Table 2. The solubility of O_2 in pure water was determined using the correlation proposed by Benson et al. (Benson et al., 1979), see Eq. (4). The same correlation is also used in this work. The concentrations of the protonated MEA and the MEA carbamate are assumed to be equal to the concentration of dissolved CO_2. A small fraction of the absorbed CO_2 will be present as carbonate or bicarbonate, but the concentrations of these species are low compared to the carbamate, especially at lower loadings.

Table 2

Model parameters for the solubility of O_2 in loaded aqueous MEA solvents. (Buvik et al., 2021; Weisenberger and Schumpe, 1996) The h_{T,O_2} parameter is valid from 273 K to 353 K.

Parameter	Unit	Value	Reference
h_{MEAH^+}	m^3·kmol^{-1}	0.0133	Buvik et al. (Buvik et al., 2021)
h_{MEACOO^-}	m^3·kmol^{-1}	0.1284	Buvik et al. (Buvik et al., 2021)
$h_{HCO_3^-}$	m^3·kmol^{-1}	0.0967	Schumpe et al. (Weisenberger and Schumpe, 1996)
$h_{G,O_2,0}$	m^3·kmol^{-1}	0	Schumpe et al. (Weisenberger and Schumpe, 1996)
h_{T,O_2}	m^3·kmol^{-1}·K^{-1}	−0.000334	Schumpe et al. (Weisenberger and Schumpe, 1996)

(Jakobsen et al., 2005) In addition, the ion-specific parameter for bicarbonate is similar to the parameter for the carbamate, so significant deviations in O_2 solubility are not expected.

$$\log_{10}\left(\frac{c_{O_2,H_2O}}{c_{O_2,l}}\right) = \sum_{i=1}^{i=n}(h_i + h_{G,O_2})c_{i,l} \tag{2}$$

$$h_{G,O_2} = h_{G,O_2,0} + h_{T,O_2}(T - 298.15) \tag{3}$$

$$c_{O_2,H_2O} = \frac{5.556 \cdot 10^4 p_{O_2}}{\exp\left(3.71814 + \frac{5596.17}{T} - \frac{1049668}{T^2}\right) - p_{O_2}} \tag{4}$$

2.3.2. Oxidative degradation kinetics

The experimental dataset on oxidative degradation of MEA in a stirred open batch reactor by Vevelstad et al. (Vevelstad et al., 2016) is used in this work to develop a degradation model. For the experiments, the reactor was filled with the loaded aqueous MEA solvent and exposed to O_2 through the bubbling of an artificial flue gas at atmospheric conditions. The concentration of O_2 in the dry gas varied from 6 vol% to 98 vol%, whereas the concentration of CO_2 was kept constant at 2 vol%, to keep the solution loaded. Most of the gas was recycled, and a small purge and make-up were used to control the gas composition. The purge gas was led through a cooler to condense volatile compounds. The temperature in the experiments varied from 55 to 75 °C.

The correlation for gas bubbles in a stirred tank by Cussler (Cussler and Cussler, 2009) is used to estimate the liquid phase mass transfer coefficient (k_{L,O_2}). The correlation is given in Eq. (5), where D_{O_2} is the diffusivity of O_2, d_b the bubble diameter, P/V the stirring power per volume, ρ_L the density, and ν_L the kinematic viscosity of the solvent. The dynamic viscosity and density of the loaded aqueous MEA solvent are calculated using the correlation by Weiland et al. (Weiland et al., 1998), and the diffusivity of O_2 has been estimated using the Wilke-Chang correlation (Geankoplis et al., 2018). Other experimental parameters, such as reactor volume (1.0 L), stirring power (12.5 W), and average bubble diameter (8 mm), were determined by analyzing the setup by Vevelstad et al. (Vevelstad et al., 2016).

The mass transfer resistance for O_2 in the gas phase is assumed to be negligible, as gas absorption processes are commonly controlled by mass transfer in the liquid (Cussler and Cussler, 2009). In addition, the concentration of O_2 in the gas bubble is assumed to be constant.

$$k_{L,O_2} = \frac{0.13 D_{O_2}}{d_b}\left(\frac{(P/V)d_b^4}{\rho_L \nu_L^3}\right)^{\frac{1}{4}}\left(\frac{\nu_L}{D_{O_2}}\right)^{\frac{1}{3}} \tag{5}$$

The equilibrium loadings were determined given the experimental temperature and CO_2 partial pressure in the wet gas using the equilibrium data by Aronu et al. (Aronu, 2011). For the experiments at 55 °C, 65 °C, and 75 °C the loading was calculated to be 0.43, 0.37, and 0.30 respectively.

The proposed reaction rate for the degradation of MEA is given in Eq. (6). The solvent is nearly always loaded to some degree in industrial capture plants and the experiments by Vevelstad et al. (Vevelstad et al., 2016), so it is not necessary to consider unloaded solvent. The CO_2 loading is assumed to influence the O_2 solubility, viscosity, and mass transfer resistance for O_2 but not the degradation kinetics. The concentration of MEA was found to influence the degradation rate (Supap et al., 2001; Kasikamphaiboon et al., 2015; Bello and Idem, 2006), and is thus included in the kinetic rate equation. Although no significant changes in MEA concentration are expected in the capture process due to solvent make-up, a decrease in MEA is observed during the batch experiments. Therefore, the concentration of MEA should be considered when developing the model.

The oxidative degradation products are not considered in this work. The oxidative reaction mechanisms and interactions between intermediates are complex and not fully understood. Without a better understanding of these mechanisms, it is hard to develop a generalized

model that can make accurate predictions of degradation product concentrations regardless of the experimental setup or process geometry. An oxidative kinetic model based on partially incorrect reaction mechanisms may perform well with respect to the data it is regressed with but may give inaccurate results when applied in a capture process, for example through the interactions between oxidative and thermal degradation products of MEA.

Instead, the consumption of MEA and O_2 is investigated. Léonard et al. (Léonard et al., 2014) proposed a weighted overall reaction balance for the oxidative degradation of MEA, in which 1.3 mol of O_2 are consumed per mole of MEA. Goff (Goff, 2005) also estimated the O_2 stoichiometry for degradation of MEA using experimental results by Rooney et al. (Rooney et al., 1998). They estimated the O_2 stoichiometry for loaded MEA (0.25 mol CO_2 per mol MEA) to be 1.44, which is comparable with the findings by Léonard et al. (Léonard et al., 2014). The developed degradation model in this work will assume a stoichiometry of 1.3. The reaction rate for the consumption of O_2 is then given in Eq. (7).

$$R_{MEA} = k_r c_{MEA} c_{O_2,L}^n \tag{6}$$

$$R_{O_2} = 1.3 \cdot k_r c_{MEA} c_{O_2,L}^n \tag{7}$$

2.3.3. Objective function and optimization

The accumulation of dissolved O_2 in the liquid bulk is equal to the transport from the gas–liquid interface minus the consumption by the degradation reaction, as expressed in Eq. (8). At steady state, the concentration of O_2 in the liquid bulk is constant and the expression can be simplified to Eq. (9), which can then be solved for $c_{O_2,L}$. The concentration of MEA in the reactor over time can then be described by Eq. (10), where the reaction rates for MEA and O_2 are given in Eq. (6) and Eq. (7), respectively. The reaction rate coefficient at the reaction temperature is set using Eq. (1). The variables that are optimized are the reaction rate coefficient at a reference temperature of 338.15 K (k_{ref}), the activation energy (E_A), and the reaction order of O_2 (n).

$$V_R \frac{dc_{O_2,L}}{dt} = a_I J_{O_2} V_R - \epsilon_L R_{O_2} V_R \tag{8}$$

$$0 = k_L a_I (c_{O_2,I} - c_{O_2,L}) - \epsilon_L R_{O_2} \tag{9}$$

$$\frac{dc_{MEA}}{dt} = R_{MEA} \tag{10}$$

The sum of square errors (SSE) with respect to the experimental results was used as the objective function. The kinetic parameters for the reaction are determined by minimizing this objective function using the particle swarm optimization implementation in MATLAB. This is a global optimizer suitable for multi-variable non-linear objective functions. The optimization was run multiple times while changing the optimization settings and initial particle distribution, and similar results were obtained each time.

2.4. Capture plant simulations

A process flow diagram of the carbon capture simulations is given in Fig. 2. The flue gas is brought in contact with the solvent in the absorber, where CO_2 is selectively removed. The rich solvent is then heated in a heat exchanger, and the CO_2 is desorbed in the stripper. The reboiler supplies the additional heat that is required for desorption. The solvent is then cooled in the heat exchanger and subsequent cooler and recycled to the absorber.

The columns are filled with a structured packing to facilitate extensive interfacial contact between the liquid and the gas. Both columns have two liquid distributors, one at the top of the packing and another one midway through. Although the distributors are not simulated, they are included in the plant model in the degradation framework. Since
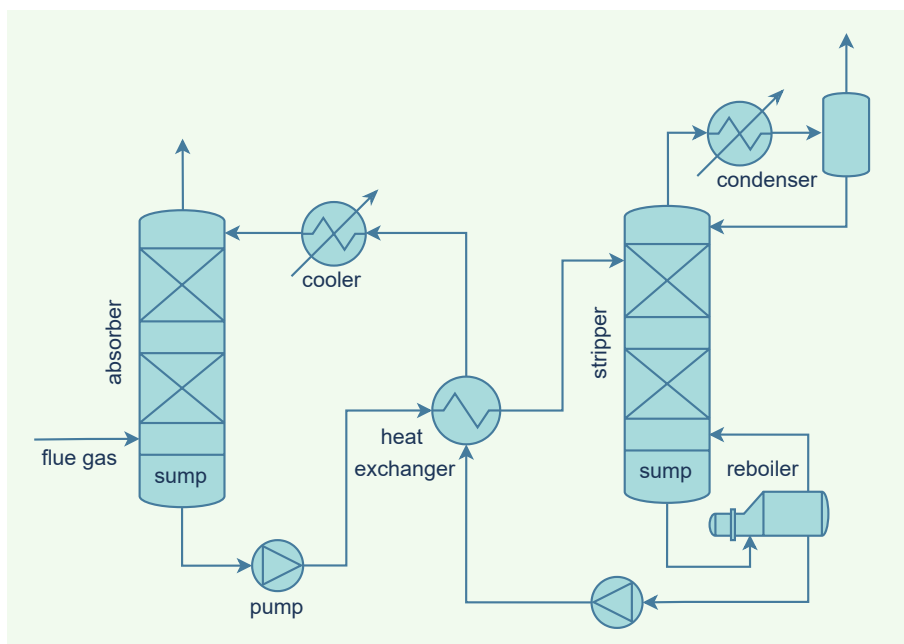
Fig. 2. Process flow diagram of the simulated carbon capture plants.

emissions are outside the scope of this work, water washes have not been simulated. Make-up streams ensure that volatile emissions of water or solvent in the treated flue gas or the CO_2 product are replaced.

Aspen Plus V10 is used in this work to simulate the capture plants. The RadFrac column model with rate–based calculations is used to simulate the absorber and stripper. Mass transfer and liquid holdup are modeled with the mass transfer correlation for structured packing by Bravo et al. (Brf-92) with reactions in the film layer. Heat transfer was modeled using the Chilton and Colburn method. The vapor is modeled as a plug flow, whereas the liquid phase is considered to be ideally mixed at each segment (VPlug). This is done to simulate maldistribution of the liquid and the effect of axial dispersion. The gas phase, on the other hand, typically maintains a uniform distribution throughout the packing (Strigle, 1987). Different segment heights were tested and finally, a height of 0.4 m was selected. This height yielded the most satisfactory result during the validation of the simulations using the data by Tobiesen et al. (Tobiesen et al., 2007; Tobiesen et al., 2008).

A plate heat exchanger was selected to facilitate heat exchange between the lean and rich solvent. The exchanger was simulated using the shortcut method with a temperature approach of 7 °C. The optimum approach temperature of heat exchangers for process streams usually lies in the range of 10 – 30 °C, but plate heat exchangers are capable of achieving lower approach temperatures (Towler and Sinnott, 2013). The calculated exchange area is used in combination with typical dimensions for plate heat exchangers (Towler and Sinnott, 2013), to determine the liquid holdup and residence time for the exchanger. A shell and tube heat exchanger was also tested, resulting in comparable residence times.

The solvent residence times in other parts of the process can vary from plant to plant but have been based on recommendations for the specific process equipment (Engineering Data Book, 2004). Residence times in piping in between process equipment have been determined using a fluid velocity of 1.0 m/s and estimated required pipe lengths. The residence times and other simulation parameters for the investigated cases are given in Table 3. Typical flue gas specifications from the literature are used to estimate the flue gas composition for a natural gas–fired power plant (Herraiz et al., 2018; Amrollahi et al., 2012), a waste-to-energy plant (Fagerlund et al., 2021; Magnanelli et al., 2021), a coal-fired power plant (Knudsen et al., 2009; Moser et al., 2020), and a cement plant (Knudsen et al., 2014). All flue gases were assumed to be saturated with water when entering the absorber. Other process

parameters, such as solvent inlet temperatures, lean loading, and column pressures, have been estimated using typical values found in literature (Freguia and Rochelle, 2003; Zhang et al., 2009; Rao and Rubin, 2002; Abu-Zahra et al., 2007).

To be able to compare degradation between the capture simulation, some process parameters have been fixed. The packing heights for the absorber and stripper were kept constant, as well as the CO_2 loading of the lean solvent and the percentage of CO_2 removed. For each flue gas case, the lean solvent flow rate was adjusted to ensure 90% of the CO_2 was removed from the flue gas in the absorber. The stripper duty was then adjusted to strip the solvent down to the specified lean loading. The simulations are not optimized for the specified flue gas because the column height and lean loading were fixed for all cases, and as a result, the energy requirements are slightly higher than those for the optimized processes.

2.5. Oxygen solubility and mass transfer in the absorber

The O_2 solubility model by Buvik et al. (Buvik et al., 2021) used for the regression of the oxidative degradation reaction kinetics from the experimental degradation results, is also used to determine the concentration of O_2 in the capture process. Similar to in the degradation experiments, mass transfer limitations for O_2 in the absorber packing may reduce the degradation rate. The impact of these mass transfer limitations was evaluated using the correlation by Billet et al. (Billet and Schultes, 1999) for the liquid phase mass transfer coefficients in structured packings on the coal-fired flue gas capture case.

Fig. 3 shows the calculated volumetric liquid-phase mass transfer coefficient as a function of the packing depth and Fig. 4 shows the influence of the mass transfer resistance on the concentration of O_2 in the absorber packing. Although, the relatively high temperatures at the top of the absorber packing lead to an increase in the mass transfer coefficient, the increase in degradation rate is even larger. Therefore, the difference between the equilibrium concentration of O_2 at the interface and the bulk concentration of O_2 is increased slightly. However, the difference between both concentrations is small throughout the column, and the bulk concentration is at least 95% of the equilibrium. Therefore, mass transfer resistances in the absorber packing can be neglected and the equilibrium solubility can be used to determine the concentration of O_2.

Table 3
Simulation parameters for the investigated industrial base cases.

	Unit	Natural gas	Waste-to-energy	Coal	Cement
Absorber					
Packing	–	Mellapak 250Y	Mellapak 250Y	Mellapak 250Y	Mellapak 250Y
Packing height	m	12.0	12.0	12.0	12.0
Pressure top	bar	1.1	1.1	1.1	1.1
Sump residence time	s	180	180	180	180
Temp. liquid inlet	°C	40.0	40.0	40.0	40.0
Temp. liquid outlet	°C	41.4	42.8	45.2	51.7
Temp. gas inlet	°C	40.0	40.0	40.0	40.0
Liquid-gas ratio	wt/wt	0.91	1.63	2.46	3.83
Flue gas CO_2	vol%	4.2	8.0	12.0	20.2
Flue gas O_2	vol%	11.8	10.5	5.0	8.6
Flue gas H_2O	vol%	6.7	6.7	6.7	6.7
Flue gas N_2	vol%	77.3	74.8	76.3	64.5
Lean loading	mol/mol	0.19	0.19	0.19	0.19
Rich loading	mol/mol	0.52	0.53	0.54	0.54
Stripper					
Packing	–	Mellapak 250Y	Mellapak 250Y	Mellapak 250Y	Mellapak 250Y
Packing height	m	10.0	10.0	10.0	10.0
Pressure condenser	bar	1.8	1.8	1.8	1.8
Sump residence time	s	180	180	180	180
Reboiler residence time	s	240	240	240	240
Temp. reboiler	°C	119.0	119.0	119.0	119.0
Reboiler duty	MJ/kg CO_2	3.62	3.50	3.46	3.47
Heat exchanger					
Exchanger type	–	Plate	Plate	Plate	Plate
Temp. approach	°C	7.0	7.0	7.0	7.0
Residence time (per side)	s	30	30	30	30

Fig. 3. Volumetric mass transfer coefficient for the liquid phase in the absorber packing as a function of the packing depth for the coal-fired power plant case.

Fig. 4. Concentration of dissolved O_2 in the liquid bulk with and without considering mass transfer limitations in the liquid phase as a function of the packing depth for the coal-fired power plant case.

including the solvent, the CO_2 content of the flue gas, and the liquid-to-gas ratio, and absorber bulge temperatures up to $70 – 80$ °C are not uncommon for processes with MEA. (Kvamsdal and Rochelle, 2008) Given the temperature dependence of the oxidative degradation reactions, the elevated temperatures in the packing are expected to lead to increased degradation.

Temperature control in the absorber packing in the form of intercooling is thus a potential degradation mitigation strategy. In this case study, the solvent is intercooled once at 2.4 m from the top of the packing, as this resulted in the lowest peak temperature in the packing. Although packings with in-situ intercooling are under development (Staab et al., 2022), the solvent is typically collected and removed from the column to be cooled down, after which it is returned. This case study initially focuses on the application of instantaneous in-situ intercooling that does not require additional solvent holdup but also discusses the effect of the additional solvent holdup in the external recycle loop for in-and-out intercooling. To investigate the potential of additional cooling, degradation in an isothermal absorber at 40 °C is also considered and evaluated.

Lower absorber temperatures can also lead to more efficient CO_2 absorption, and thus lower requirements for the column height, solvent flow rate, and/or reboiler duty. These effects have not been modeled. The column height, reboiler duty, solvent flow rate, and lean loading have thus been set according to the values in the reference case.

2.6. Case studies

The coal–fired power plant case presented in section 2.4 was used as the starting point for all case studies, focusing on the impact of process and solvent modifications on the predicted MEA degradation rate. The coal–fired power plant case was chosen as a reference case because the degradation in the coal case was diverse, with significant contributions from direct oxidative degradation, degradation by dissolved O_2, and thermal degradation. The case studies and the assumptions made are described briefly in the sections below.

2.6.1. Intercooled and isothermal absorbers

The absorber packing is expected to be one of the locations where oxidative degradation occurs since the solvent is in direct contact with O_2 from the flue gas. The exothermic nature of CO_2 absorption causes the temperatures in the absorber to increase and leads to a temperature bulge. The magnitude of this bulge is dependent on a number of factors,
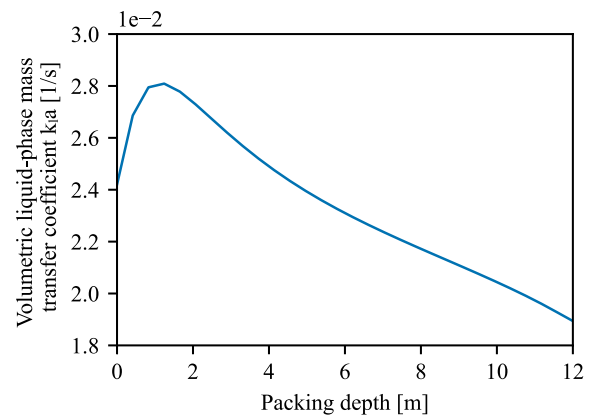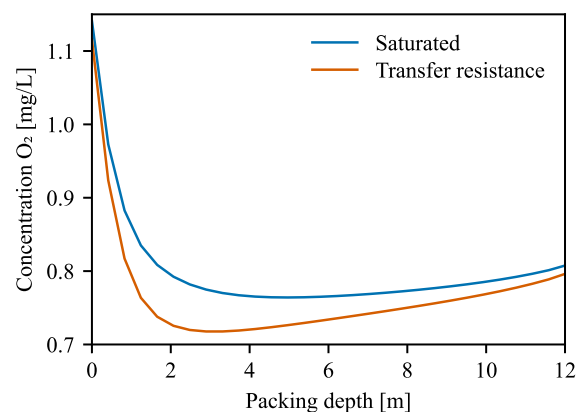
2.6.2. Dissolved oxygen removal

Oxidative degradation can occur even when the solvent is no longer

exposed to O_2 in the flue gas. The rich solvent may contain O_2 that was dissolved in the absorber, which can lead to indirect oxidative degradation of the solvent. This type of degradation is expected to occur in the absorber sump, heat exchanger, and piping until the O_2 is desorbed in the stripper. The extent of this type of degradation depends on the O_2 content of the flue gas, the solubility of O_2, and the oxidative degradation rate. The removal of dissolved O_2 from the solvent may be an effective method for reducing this indirect degradation (V. Figueiredo et al., 2021).

This removal of dissolved O_2 can be achieved using membrane contactors. Figueiredo et al. (V. Figueiredo et al., 2021) investigated the potential of such a removal technology and concluded that removal efficiencies up to 90% are feasible using a dense layer membrane with a 30 wt% MEA solvent. Alternatively, dissolved O_2 can be removed by sparging the rich solvent with nitrogen in the absorber sump or right after the absorber in a separate column. Bench-scale experiments by Nielsen showed that nitrogen sparging could reduce oxidative degradation or piperazine (PZ) by 50%. (Nielsen, 2018) Modeling work by Wu (Wu, 2022) showed that removal efficiencies up to 90% are feasible when applying nitrogen stripping in 5 mol/kg piperazine.

This case study investigates the potential of dissolved O_2 removal to mitigate degradation. The concentration of dissolved O_2 is reduced by 90% before the solvent enters the absorber sump. It is likely that the concentration of O_2 is higher in some parts of the sump in case of nitrogen sparging, or that additional holdup volume is required for O_2 removal using membranes, but these effects are not considered in the case study.

2.6.3. Change in capture efficiency

Amine-based capture processes can operate with various CO_2 capture efficiencies, and operation at lower or higher capture efficiencies than 90% is possible. Therefore, in this case study, the reference case was modified to remove both 95% and 85% of the CO_2 in the flue gas. For the 95% efficiency case, the packed height was increased from 12 to 15 m, and an additional solvent redistributor was added. In addition, the solvent flow rate was increased by 5.6% to ensure the same amount of solvent is available per mole of captured CO_2 and the rich loading is the same as in the reference case. For the process with an 85% capture efficiency, the packed height was reduced to 10 m and the solvent flow rate was reduced by 5.6%.

2.6.4. Stripper pressure

The energy that is required for stripping the CO_2 is supplied in the reboiler in the form of pressurized steam. The energy is used for sensible heating, producing water vapor, and driving the endothermic CO_2 desorption reaction. The pressure in the stripper typically is between 1.5 bar and 2.0 bar (Warudkar et al., 2013), and the base case simulations in this work are run with a pressure of 1.8 bar. An increase in stripper pressure will lead to an increase in operating temperature. Higher temperatures favor the desorption of CO_2 and result in higher partial pressures of CO_2 at the same loading. Therefore, less water vapor is needed to facilitate the desorption and less energy is required in the reboiler (Warudkar et al., 2013; Puxty and Maeder, 2016). A downside of higher temperatures in the stripper, especially in the sump and reboiler, is the increased rate of thermal degradation.

In this case study, the reboiler pressure is varied between 1.3 bar and 3.0 bar. The reboiler duty is adjusted to ensure 90% of CO_2 is stripped, and the lean loading and solvent flow rate remain unchanged. Since the volumetric flow rate of the gas changes with pressure, the diameter of the stripper is adjusted to ensure that the stripper is operated at 75% flooding.

2.6.5. Reduced solvent residence times

Solvent holdup is required throughout the process to facilitate mass and heat transfer, and buffer tanks are required for stable operation of the capture plant. The sump, for example, collects the solvent that exits

the packing, forms an inventory buffer for the pump, and prevents it from running dry. The residence time can, from a degradation perspective, also be regarded as an exposure time in which the solvent is exposed to increased temperatures or environments containing O_2. A reduction of this exposure time may thus reduce degradation. Therefore, several of the equipment residence times have been reduced by 50% in this case study. An overview of the default and reduced residence times is given in Table 4. Solvent degradation is then predicted and evaluated.

2.6.6. Oxygen content in the flue gas

The concentration of O_2 in the flue gas is expected to influence the oxidative degradation rates in the process since the solubility of O_2 is proportional to its partial pressure in the gas phase. The studied industrial flue gases given in Table 3 have different concentrations of O_2 and CO_2. The concentration of CO_2 has a significant impact on process conditions, such as rich loadings or the temperature profile in the absorber, and will thus influence the degradation rate. This case study aims to isolate and study the effect of the O_2 concentration in the coal-fired flue gas of the reference case. The concentration of O_2 is varied from 0.1% to 12%, while the concentration of CO_2 and H_2O are kept constant. The remainder of the gas is set to be N_2.

2.6.7. Reduced oxidative degradation rate

In the context of solvent degradation, MEA is the most tested and studied amine. (Gouedard et al., 2012) Despite its wide-spread interest and use, the amine is not known for its stability towards oxidative degradation and other solvent candidates have been found to be more resilient, for example, MDEA, PZ, and AMP. (Voice et al., 2013) However, experimental data on degradation of these alternative solvents is limited. Extended datasets that are similar in size and detail to the dataset by Vevelstad et al. on 30 wt% MEA are not available, making it more challenging to develop kinetic degradation models for these solvents. Therefore, in this case study, the kinetic parameters in the oxidative degradation model for MEA are varied, and the effect on degradation in the process is investigated.

Besides the resilience towards oxidative degradation, there are more differences in the properties of solvents used for carbon capture. These properties can significantly influence process parameters such as temperatures in the absorber, solvent capacity and flow rates, and O_2 solubility. This case study does not consider these effects and thus only gives a hypothetical overview of the expected behavior of more stable solvents.

2.7. Validation of the simulations

The simulations in Aspen Plus are validated using experimental data by Tobiesen et al. (Tobiesen et al., 2007; Tobiesen et al., 2008) on the CO_2 capture performance of a Mellapak 250Y packing in the packed absorber and desorber sections. The experimental data were obtained from a 3-month campaign in a laboratory pilot plant. Although the columns were relatively small, 4.36 m for the absorber and 3.89 m for the stripper, experiments were conducted with varying temperatures, flow rates, and lean and rich loadings to simulate the different operating conditions in the various sections of the packed columns.

For the absorber, the simulations give an accurate representation of

Table 4
Default and reduced residence times in the capture plant equipment.

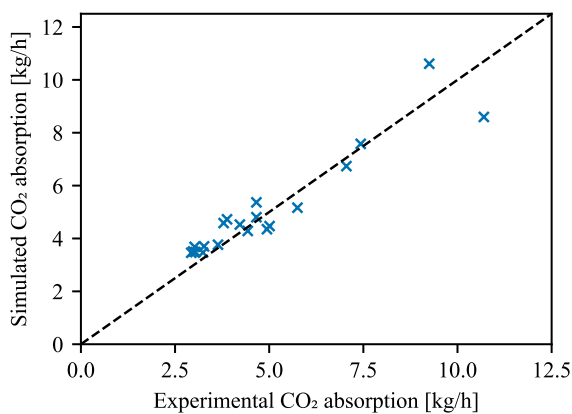| Equipment	Default residence time [s]	Reduced residence time [s]
Column distributor	15	7.5
Column sump	180	90
Reboiler	240	120
Heat exchanger	30	15
Pump	10	5
Heater and cooler	30	15

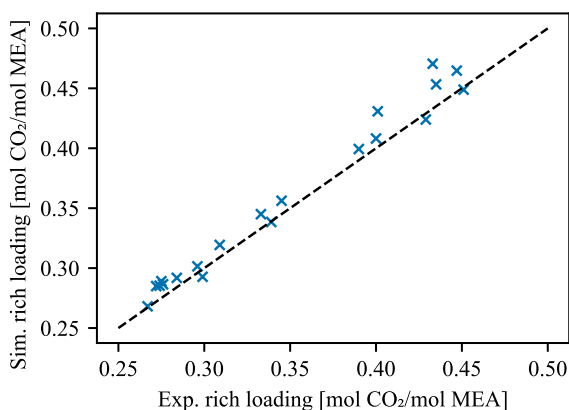**Fig. 5.** Parity plot of the experimental and simulated CO_2 absorption rate.

Fig. 6. Parity plot of the experimental and simulated rich loading of the exiting solvent.
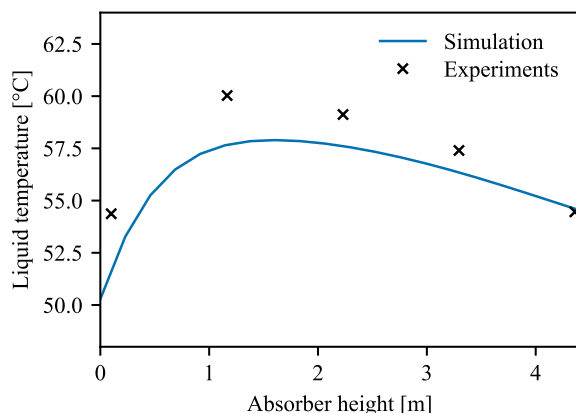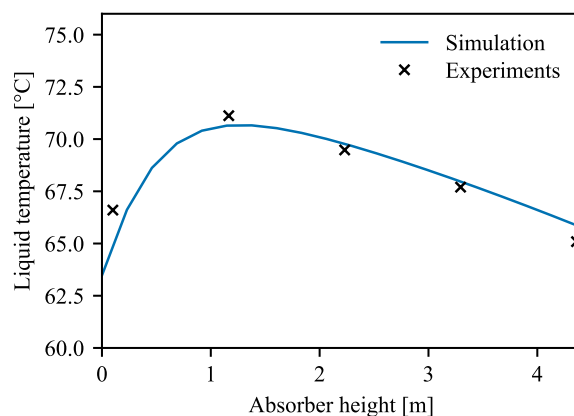

Fig. 7. Comparison between the liquid phase absorber temperature profile simulated in this work and experimental data for run 12 by Tobiesen et al. (Tobiesen et al., 2007).
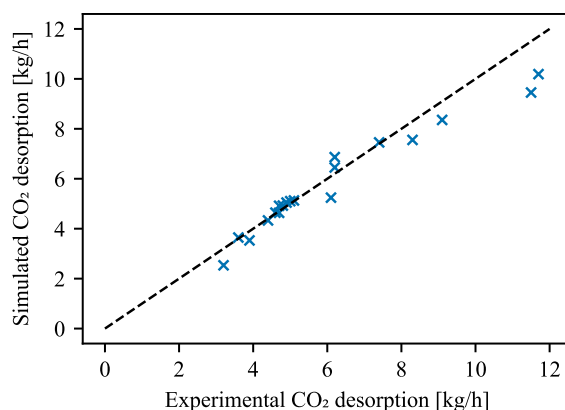

Fig. 8. Comparison between the liquid phase absorber temperature profile simulated in this work and experimental data for run 15 by Tobiesen et al. (Tobiesen et al., 2007).

Fig. 9. Parity plot of the simulated CO_2 desorption rate and the experimental results by Tobiesen et al. (Tobiesen et al., 2008).
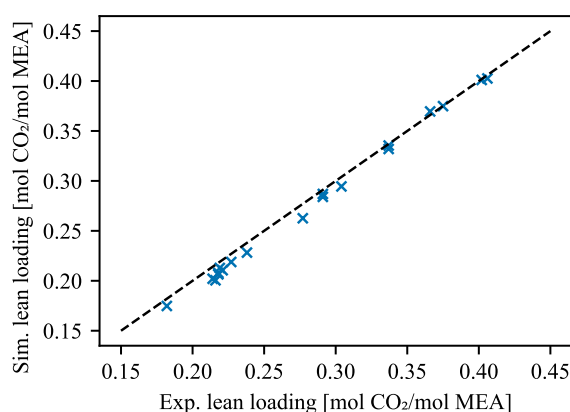
Fig. 10. Parity plot of the simulated lean CO_2 loading and the experimental results by Tobiesen et al. (Tobiesen et al., 2008).

the experiments, as can be seen in the parity plots for the absorption rate and rich loading in Fig. 5 and Fig. 6. The mean average deviations were 6.0% and 3.3% for the absorption rate and rich loading, respectively. These deviations are of the same magnitude as the deviations observed by Tobiesen et al. (Tobiesen et al., 2007).

The simulated temperature profiles in the absorber also correspond well with the experimental results, as shown in Fig. 7 and Fig. 8. In some cases, there was a slight over or under–prediction of the temperature profile, even though the absorption rate corresponded well. An example of this is the temperature profile of run 12 in Fig. 7. A reason for this

deviation may be the water content of the gas, which was not analyzed in the experiments. Tobiesen et al. (Tobiesen et al., 2007) showed that a difference in water content can significantly change the temperature profile through changes in water evaporation rates and CO_2 partial pressure, because the dry gas composition was analyzed.

The parity plots for the performance of the desorber section are given in Fig. 9 and Fig. 10. These show that there is also a good agreement between the simulation and the experimental results for the desorber. Deviations were in the same order of magnitude as for the absorber and
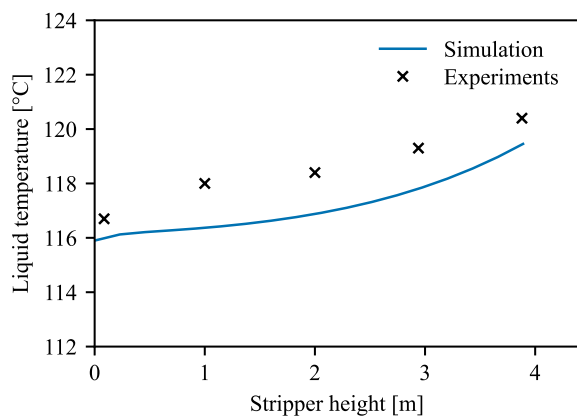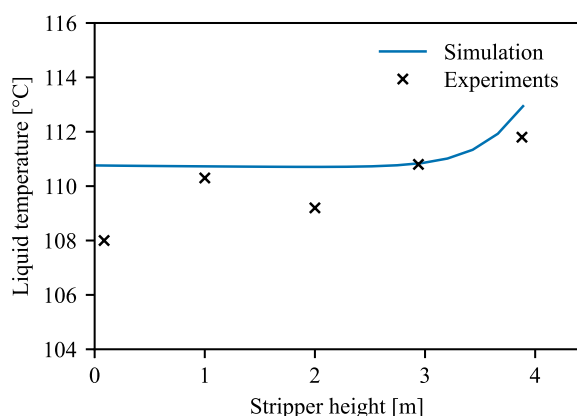
Fig. 11. Comparison between the liquid phase stripper temperature profile simulated in this work and experimental data for run 2 by Tobiesen et al. (Tobiesen et al., 2008).

Fig. 12. Comparison between the liquid phase stripper temperature profile simulated in this work and experimental data for run 18 by Tobiesen et al. (Tobiesen et al., 2008).

are considered to be acceptable.

A pair of simulated and experimental temperature profiles in the desorber is given in Fig. 11 and Fig. 12. The temperature in the stripper was difficult to measure and led to possible uncertainties in the experimental results. Firstly, it is not known which phase is in contact with the temperature sensor at any time. Also, Tobiesen et al. (Tobiesen et al., 2008) suspect that in case of high loadings, some of the liquid may flash before entering the stripper column, underestimating the enthalpy content of the flow. Despite some slight deviations in temperature, the simulations correspond relatively well with the experimental data.

3. Results

3.1. Oxidative degradation model fitting results

The fitted reaction rate coefficients and their 95% confidence intervals are given in Table 6. The reaction order with respect to O_2 is fractional, which indicates that oxidative degradation is most likely a chemical chain reaction. (Arnaut, 2021) This is in agreement with mechanisms discussed by Goff et al. (Goff and Rochelle, 2004) and Sexton (Sexton, 2008), in which free radicals derived from O_2 play a role as intermediates in oxidative degradation reactions.

The activation energy for the reaction is higher than those regressed by other works in the literature, which are 41.7 kJ/mol by Léonard et al. (Léonard et al., 2014) and 29.4 kJ/mol by Supap et al. (Supap et al., 2009). This difference may be the results of both literature works assuming that the concentration of dissolved O_2 was in equilibrium,

Table 5

Degradation reactions and reaction rate equations for the oxidative degradation model. The reference temperature for the oxidative rate coefficients is 338.15 K.

Reaction	Reaction rate [mol/m^3/s]	Reaction rate coefficient
MEA + 1.3O_2 → Prod.	$R = k_r[\text{MEA}][O_2]^n$	$k_r = k_{ref} \cdot \exp\left(\frac{-E_A}{R_{id}}\left(\frac{1}{T} - \frac{1}{T_{ref}}\right)\right)$

Table 6

Regressed reaction rate parameters for the oxidative degradation model.

Parameter	Unit	Value	95% confidence interval
k_r	(m^3/mol)^n/s	$6.790 \cdot 10^{-7}$	$[0.588 \cdot 10^{-7} - 0.784 \cdot 10^{-7}]$
E_A	J/mol	$7.908 \cdot 10^4$	$[6.952 \cdot 10^4 - 8.997 \cdot 10^4]$
n	–	0.469	$[0.405 - 0.533]$

neglecting the mass transfer resistance of O_2. The importance of this mass transfer resistance depends on the reaction rate in the liquid phase and thus on the temperature. At increased temperatures, the mass transfer can cause the actual liquid bulk concentration of O_2 to drop below the equilibrium concentration. If this is not considered, the reaction rate coefficient is underestimated, and the temperature dependency of the apparent reaction rate coefficient is smaller.

This effect can be amplified by the reaction order of O_2 since a change in O_2 concentration will result in a larger change in reaction rate coefficient in case the reaction order is high. The regressed reaction orders were reported to be 1.46 by Léonard et al. (Léonard et al., 2014) and 2.91 by Supap et al. (Supap et al., 2009). The temperatures in the degradation experiments by Vevelstad et al. (Vevelstad et al., 2016) were low compared to the typical temperatures used by Léonard et al. (Léonard et al., 2014) and Supap et al. (Supap et al., 2009). Therefore, it is also a possibility that a difference in reaction mechanism at increased temperatures leads to a lower temperature dependency of the reaction. The difference in reaction order for O_2 and the use of different O_2 solubility models makes it challenging to compare reaction rate coefficients between these studies and the current work.

The experiment at 55 °C and 21 vol% O_2 was run three times by Vevelstad et al. (Vevelstad et al., 2016), and the replicate measurements can give an insight into the uncertainty of the experiments. The absolute differences between the three runs are limited, and the standard deviation of the measured concentration of MEA is only 132.0 mol/m^3. However, it is expected that the uncertainty in the experiments is proportional to the extent of degradation, which was also the case for thermal degradation experiments (Braakhuis and Knuutila, 2021). The standard deviation of the experiments with more degradation will thus likely be higher.

One could consider the error to be proportional and evaluate the standard deviation with respect to the measured degradation, but this is also challenging due to limited degradation at 55 °C. The standard deviation for the replicates is, on average 49.7% of the measured degradation of MEA. This high error is a result of the relatively large size of the analytical error and deviations in the mass balance with respect to the measured degradation. The impact of these uncertainties will be lower for experiments with more degradation, resulting in a lower relative error.

It is thus challenging to estimate the uncertainty of the experimental data and evaluate the quality of the fit. The residual plots for the fitted model with respect to the experimental data are given as a function of

the temperature, partial pressure of O_2, degradation time, and the initial and final concentration of MEA in Figs. 13–16 through Fig. 17. The standard deviation of the model with respect to the experimental data is 248.8 mol/m^3, which is, on average 23.7%, with respect to measured degradation. Despite the deviation, the model appears to give a good representation of the experimental data, and no significant residual trends were observed. The use of additional parameters in the rate equation, for example, a reaction order for MEA, did not significantly improve the fitting results.

Fig. 18 shows the degree of saturation for O_2 in the liquid bulk with respect to the solubility at the bubble interface, where the gas and liquid phases are assumed to be in equilibrium. At lower temperatures, consumption of O_2 by the degradation reactions is relatively low, and degradation is not limited by mass transfer. As a result, the bulk concentration of O_2 is close to the equilibrium concentration. At higher temperatures, O_2 consumption in the liquid is increased, and more O_2 has to be transferred to the liquid phase. A more significant driving force is needed across the boundary layer, which causes the bulk concentration of O_2 to decrease. In these conditions, the degradation rate is partially limited by mass transfer.

Experiments with lower O_2 partial pressures are also more mass transfer limited. This is an effect of the reaction order of O_2 in the degradation reaction. The fitted reaction order is 0.47, so an increase in the concentration of dissolved O_2 will have a progressively smaller impact on the degradation rate. The O_2 solubility and the driving force over the mass transfer film, on the other hand, scale more linearly with the partial pressure of O_2 in the gas.

3.2. Predicted degradation in the industrial flue gas cases

The predicted solvent degradation for the industrial flue gas cases is given in Fig. 19. Note that the degradation rates are normalized with respect to the amount of CO_2 captured, so the absolute degradation rates are more significant for the cases with higher CO_2 concentrations in the flue gas. The degradation rates and process conditions in the absorber packing are given in Fig. 20 to Fig. 24. Degradation in the collectors and distributors is not displayed in these profiles but has been included under the absorber packing category in the bar plot in Fig. 19. The total degradation rates for the natural gas and waste-to-energy are comparable, at around 110 g MEA/ton CO_2. Degradation in the cement case was relatively high, at 150 g MEA/ton CO_2, and the lowest degradation was observed in the coal case, at 89.1 g MEA/ton CO_2.

In comparison, the total solvent losses in the capture pilot plant at Niederaussem for a coal-fired power plant, which had a similar coal flue gas composition as the case simulated in this work, were around 210 g MEA/ton CO_2 at the start of the campaign (Moser et al., 2020). Moser et al. (Moser et al., 2020) reported that losses of MEA in the gas downstream of the absorber were negligible with respect to the overall
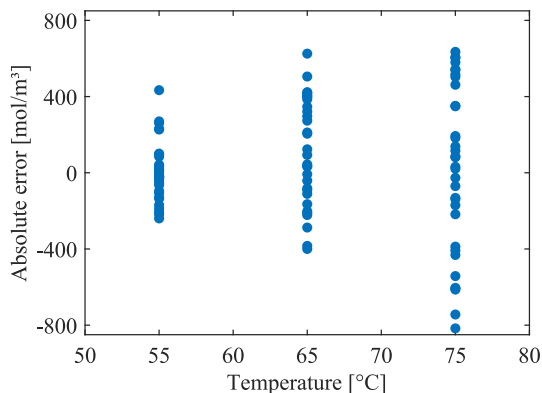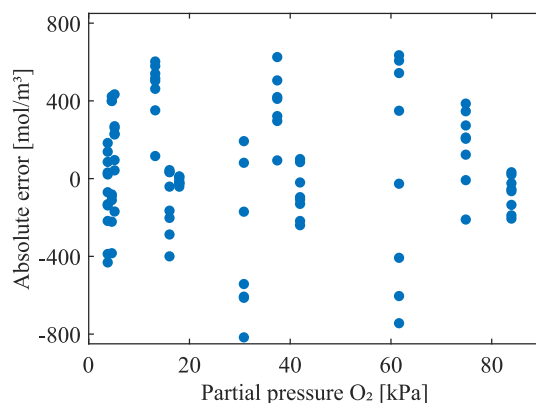
Fig. 14. Residuals of the modeled MEA concentrations with respect to the experimental values as a function of partial pressure of O_2.
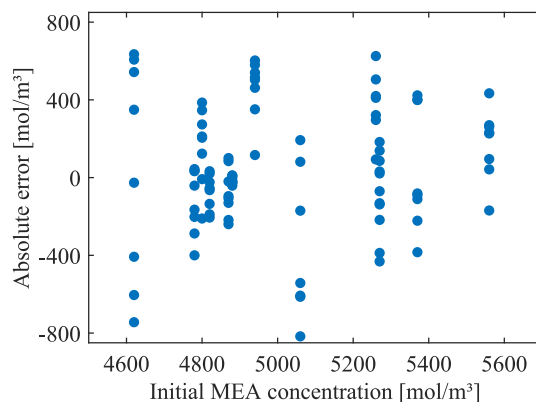
Fig. 15. Residuals of the modeled MEA concentrations with respect to the experimental values as a function of the initial concentration of MEA.
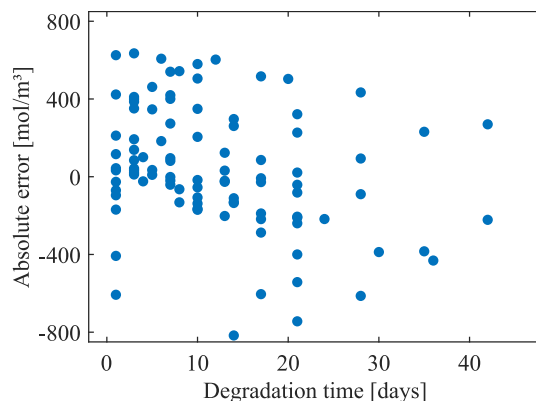
Fig. 16. Residuals of the modeled MEA concentrations with respect to the experimental values as a function of degradation time.

solvent losses and that degradation was the main cause. The predicted degradation rate is thus significantly lower than the observed degradation. This may be a result of differences in the process, for example, an increased solvent holdup, higher temperatures in the absorber, or a higher stripper pressure. In addition, the catalytic effect of dissolved iron on oxidative degradation is not modeled. Although the concentrations of iron were low at the start of the campaign (Moser et al., 2020), the catalytic effect of iron can still be significant (Chi, 2000).

Oxidative degradation seen in this work constitutes around 80% to 90% of the total degradation. The remainder is caused by thermal
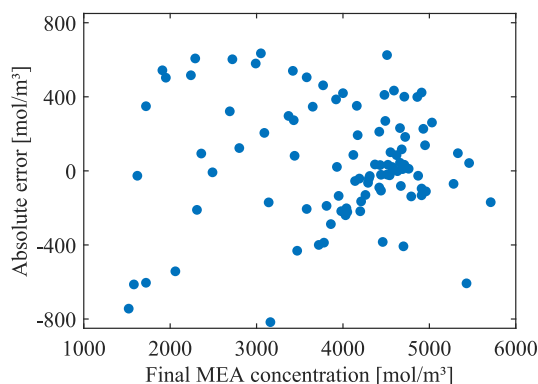
Fig. 13. Residuals of the modeled MEA concentrations with respect to the experimental values as a function of temperature.

Fig. 17. Residuals of the modeled MEA concentrations with respect to the experimental values as a function of the final concentration of MEA.
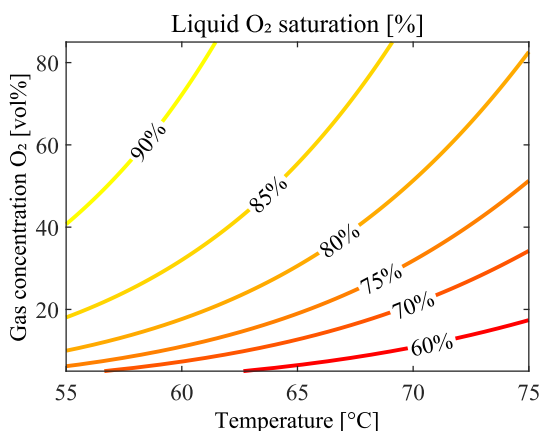

Fig. 18. Estimated liquid-phase O_2 saturation (bulk over interfacial concentration) in the experiments by Vevelstad et al. (Vevelstad et al., 2016) at various temperatures and gas-phase O_2 concentrations.
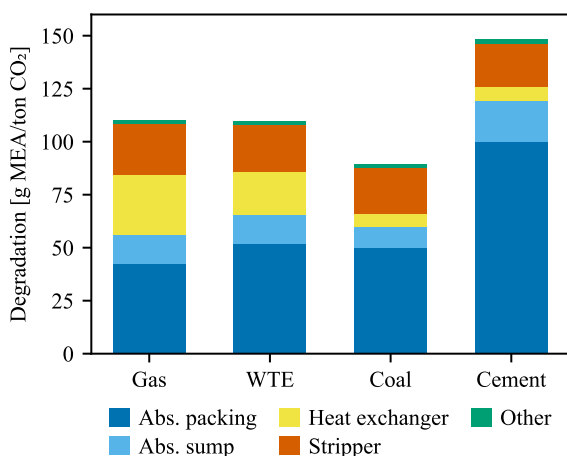

Fig. 19. Predicted MEA degradation in different parts of the capture plant for the industrial flue gases.

degradation. This is in line with the observations on degradation of MEA in experimental works and pilot plant reports in literature (Moser et al., 2020; Vevelstad et al., 2017; Lepaumier et al., 2011). Thermal degradation primarily takes place in the stripper sump and reboiler and only approximately 10% of the thermal degradation is predicted to occur in the packing and distributors in the stripper.

Léonard et al. (Léonard et al., 2015) predicted degradation in the
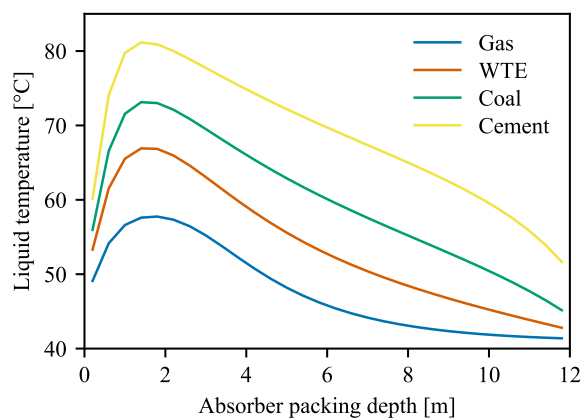
Fig. 20. Liquid temperature profiles in the absorber packing for the studied flue gas cases.

pilot plant campaign by Knudsen et al. (Knudsen et al., 2011). The composition of the flue gas was similar to the composition of the flue gas for the coal–fired power plant in this work. The concentration of CO_2 and O_2 were 14 vol% and 6 vol%, respectively. The total degradation in the pilot plant was predicted to be 79.5 g MEA/ton CO_2, which is close to the degradation predicted in this work. Léonard et al. (Léonard et al., 2015) predicted slightly more degradation in the absorber compared to the current work. This is due to increased solvent holdup since a packed height of 20 m was used, in contrast to the 12 m used in this work.

The predictions for thermal degradation by Léonard et al. (Léonard et al., 2015) are several orders of magnitude smaller. This is unexpected because the used rate equations for thermal degradation of MEA are comparable to the ones used in this work (Braakhuis and Knuutila, 2021). It could be that the stripper sump and or reboiler have not been considered in the model by Léonard et al. (Léonard et al., 2015), but even when just considering thermal degradation in the stripper packing, significantly more degradation is predicted in this study.

Degradation in the absorber is primarily oxidative and makes up a significant fraction of the total degradation for each of the processes. Higher temperatures in the absorber packing lead to more degradation. This applies to the cement case, where the high concentration of CO_2 in the flue gas leads to increased temperatures in the absorber. Based on the oxidative degradation kinetics, a stronger temperature dependence is expected, but a reduction of O_2 solubility at higher temperatures reduces the actual impact.

A higher concentration of O_2 in the flue gas also results in increased degradation. This applies to the natural gas case, in which there is significant degradation in the packing, regardless of the milder temperatures. The combination of these effects leads to comparable degradation rates in the absorber packing for the natural gas, waste-to-energy, and coal cases, despite different flue gas compositions. This can be seen in Fig. 24.

The impact of CO_2 loading on O_2 solubility is illustrated in Fig. 23. At the top of the absorber packing, the solvent is relatively lean, and the concentration of dissolved O_2 is high. The solubility is reduced as the temperature rises in the top part of the absorber packing and the CO_2 loading is increased, thereby increasing the concentrations of the protonated MEA, MEA carbamate, and carbonate ions. After the temperature peak, the concentration of dissolved O_2 is relatively constant. Here, the decrease in temperature and increase in CO_2 loading roughly balance each other out.

The liquid holdup per cubic meter of total absorber volume for each of the investigated cases is shown in Fig. 21. The flue gas flow rates are identical across all cases, resulting in equivalent column diameters and total internal volumes. Flue gases with a higher CO_2 content, such as in the cement and waste-to-energy cases, require higher liquid flow rates to achieve the required capture efficiency, which results in increased liquid
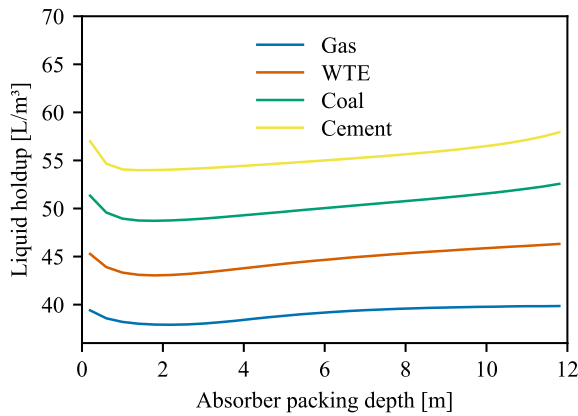
Fig. 21. Liquid holdup profiles in the absorber packing per m³ of total column volume for the studied flue gas cases.

holdup in the packing. The liquid holdup is relatively constant throughout the absorber packing. The CO_2 loading in the absorber is shown in Fig. 22.

Most of the degradation in the heat exchanger is on the rich side through indirect oxidative degradation. Although there is no direct source of O_2 in the heat exchanger, O_2 that is dissolved in the absorber reacts with the amine when the temperature is increased. A high O_2 solubility is therefore associated with more degradation in the heat exchanger. This is observed in the natural gas case, where indirect degradation in the sump and heat exchanger accounts for around 40% of the total degradation. Oxygen consumption in the rich solvent is shown in Fig. 25. It should be noted that the reaction kinetics are extrapolated to evaluate degradation at temperatures above 75 °C, which could lead to uncertainty. However, even when degradation in the hot rich stream is evaluated at 75 °C, complete consumption of dissolved O_2 is observed, so the results should not change significantly.

Because all of the dissolved O_2 has reacted before the rich solvent enters the stripper, there is no oxidative degradation in the stripper. The extent of degradation in the stripper is approximately the same for each case, due to comparable process conditions in the stripper. The holdup volumes in the stripper and reboiler, and thus also the degradation of MEA, are proportional to the amount of CO_2 removed. A slightly higher relative degradation rate is observed in the stripper for the natural gas capture process. This is caused by the relatively low concentration of CO_2 in the flue gas, which results in a lower rich loading and a reduced cyclic capacity, as the lean loading is fixed. As a result, the solvent flow rate and, thus, the solvent holdup volumes are increased slightly. Degradation in other parts of the plant, such as the pumps and piping, is negligible for all the studied base cases.
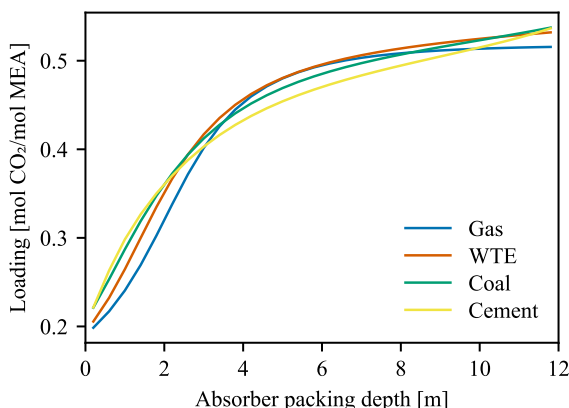

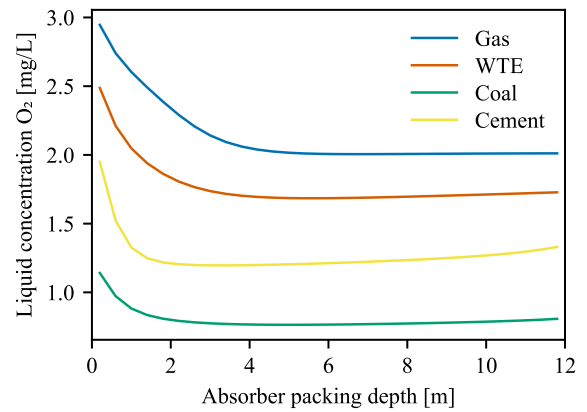**Fig. 22.** Loading in the absorber packing for the three base cases.

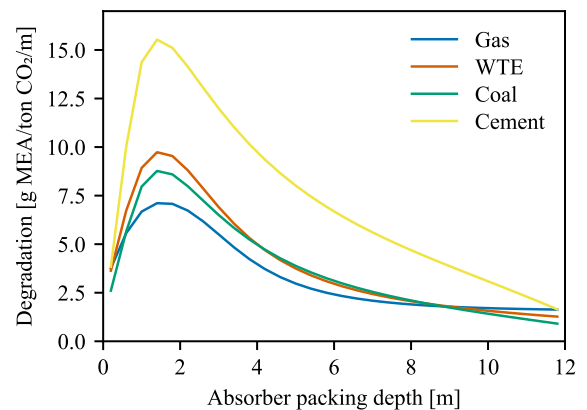**Fig. 23.** Dissolved O_2 in the absorber packing for the three base cases.

Fig. 24. Predicted MEA degradation in the absorber packing per meter of packing for the three base cases.
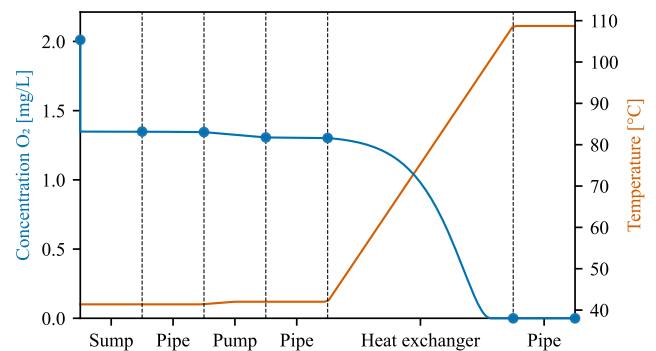

Fig. 25. Liquid temperature and predicted concentration of dissolved O_2 in the rich solvent from the absorber sump to the inlet of the stripper for the natural gas-fired power plant capture case.

3.3. Impact of process modifications

The predicted degradation of MEA for each of the process modifications is given in Fig. 26. The degradation in the coal-fired power plant base case is used as a reference. Each case is discussed in more detail below.

3.4. Intercooled and isothermal absorber

Fig. 26 shows that the predicted degradation is significantly lower for the in-situ intercooled and isothermal cases. The largest reduction in degradation is observed in the absorber packing. The temperature
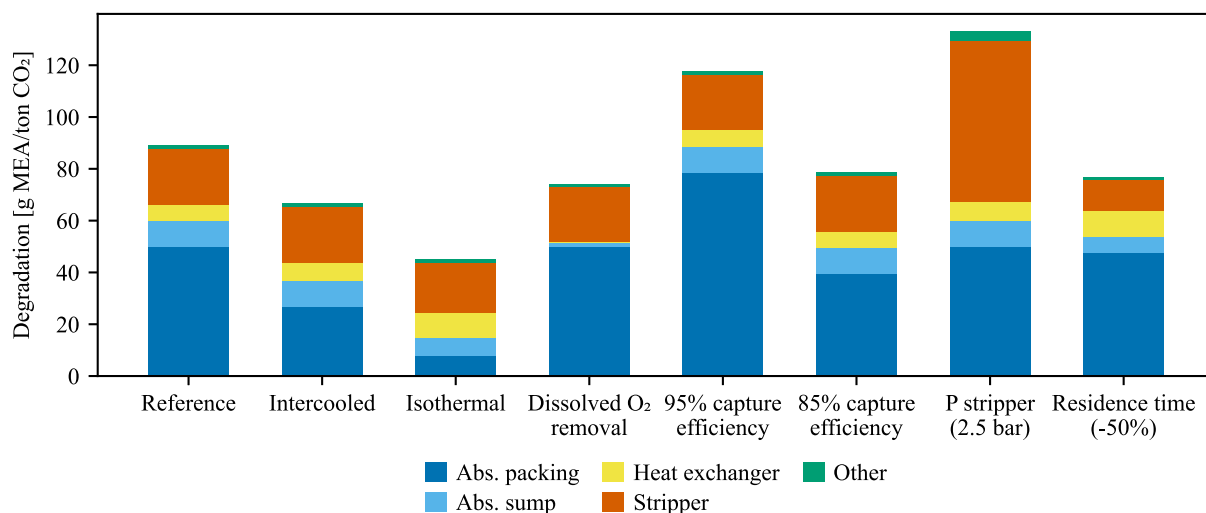
Fig. 26. Predicted degradation of MEA for the process modifications to the coal–fired power plant base case, which is given here as a reference.

profiles and degradation rate profiles in the absorber packing for the reference, intercooled, and isothermal cases are given in Fig. 27 and Fig. 28, respectively. Intercooling in the absorber is an effective method to reduce both the peak temperature and the overall temperatures in the absorber packing. As a result, the degradation in the packing is reduced by 44%. Additional heat removal from the absorbent influences the degradation rates significantly, since the isothermal case shows an 71% reduction in degradation in the entire absorber compared to the reference case.

The loading profiles and the concentration profiles of dissolved O_2 in the absorber packing are shown in Fig. 29 and Fig. 30, respectively. The isothermal case shows that the CO_2 loading has a significant impact on the solubility O_2. Although the CO_2 loadings in the isothermal absorber packing are generally higher, the concentrations of dissolved O_2 are also higher. This indicates that the effect of temperature is more prominent. The lower temperature in the bottom of the absorber for the isothermal case reduces the degradation rate in the sump. The remaining dissolved O_2 now reacts in the heat exchanger instead, resulting in an increase in degradation in this part of the plant. The total amount of degradation as a result of dissolved O_2 is increased slightly due to a higher O_2 solubility in the sump.

In this comparison, the column height, solvent flow rate, lean loading, and reboiler duty remain unchanged. In reality, increased absorption rates due to intercooling may impact some of these process parameters. For example, shorter columns may be used to capture the same amount of CO_2, thus reducing the solvent holdup and exposure
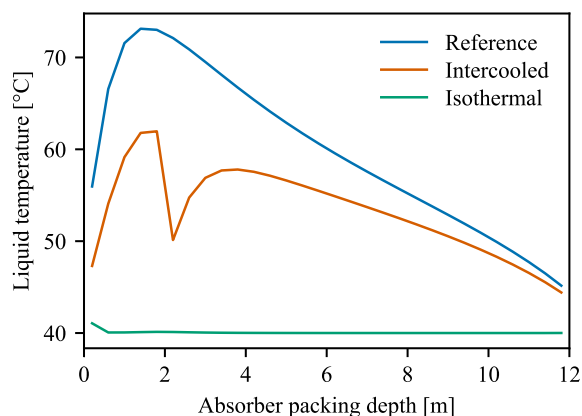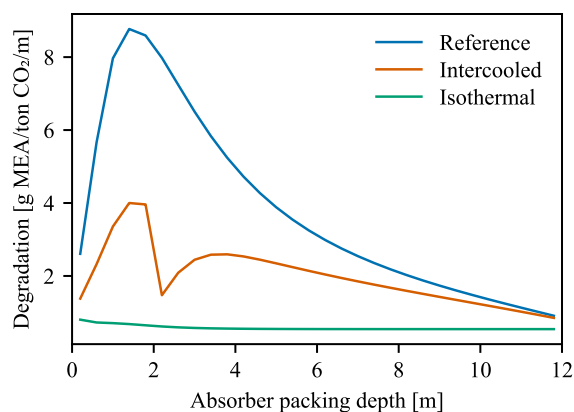

Fig. 28. Degradation rate per ton of CO_2 captured per meter of packing height in the absorber packing for the reference, intercooled, and isothermal cases.
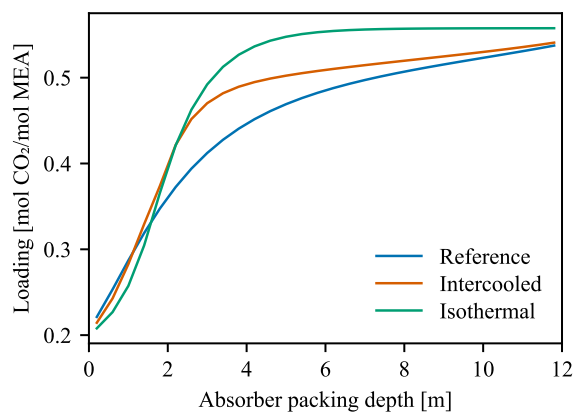

Fig. 29. Liquid CO_2 loading in the absorber packing for the reference, intercooled, and isothermal cases.

time in the absorber packing. Alternatively, intercooling may lead to higher rich loadings and increase the cyclic capacity. This would lead to lower solvent flow rates and reduced holdups not only in the absorber but also in the stripper and other parts of the plant.

In the more realistic scenario of in-and-out intercooling, where the solvent is temporarily removed from the column, additional solvent holdup is expected to be required. The solvent has to be collected,
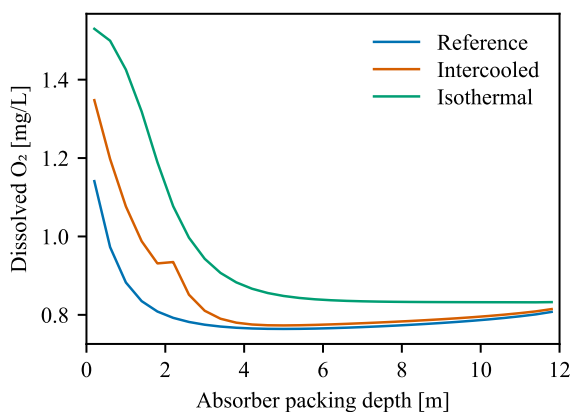

Fig. 27. Liquid temperature in the absorber packing for the reference, intercooled, and isothermal cases.

Fig. 30. Liquid O_2 concentration in the absorber packing for the reference, intercooled, and isothermal cases.

Fig. 32. Liquid temperature and predicted concentration of dissolved O_2 in the in-and-out intercooling loop.

transported, cooled, transported, and redistributed in the absorber again. To study the impact of this addition to the process, the simulation is adjusted to include the intercooling loop, as shown in Fig. 31. Solvent is removed at a height of around 10 m in this case and is transported to the ground to be cooled in a heat exchanger and re-entered into the absorber at approximately the same height as the outlet. The residence time of the intercooling loop is estimated to be around 40 s.

The solvent is saturated with O_2 when leaving the column, and some of the dissolved O_2 is consumed in the intercooling loop. This can be seen in Fig. 32, which shows the concentration of O_2 and the temperature of the solvent in the intercooling loop. Some of the dissolved O_2 is consumed by the oxidative degradation reactions, in particular before the solvent is cooled. After cooling, degradation is limited.

An overview of the predicted degradation rates in the simulated processes for the reference and intercooled cases is given in Table 7. The initial case study on ideal intercooling is predicted to have a degradation rate of 36.7 g MEA/ton CO_2 in the absorber, which is a reduction of 39.0% with respect to the reference case. The total degradation in the entire process is reduced by 25.0%. The implementation of in-and-out intercooling is predicted to add 9.3 g MEA/ton CO_2 of additional degradation, resulting in a total degradation of 76.1 g MEA/ton CO_2, which is only a reduction of 14.6% with respect to the base case. This shows that there is a significant potential for intercooling to reduce degradation, but that the implementation is important, and that additional solvent holdup and residence times have to be minimized.

3.4.1. Dissolved oxygen removal

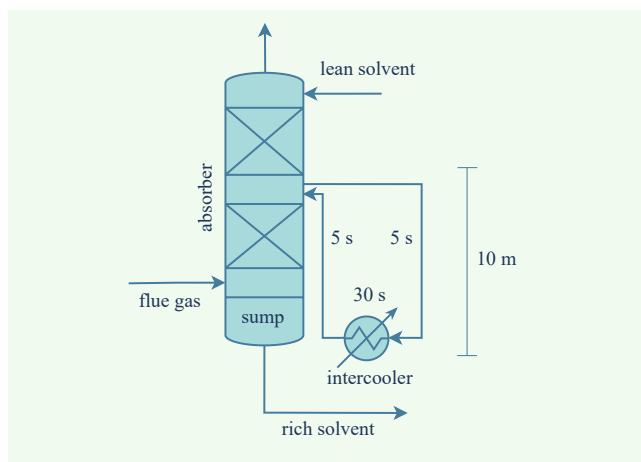The 90% removal of dissolved O_2 before the solvent enters the

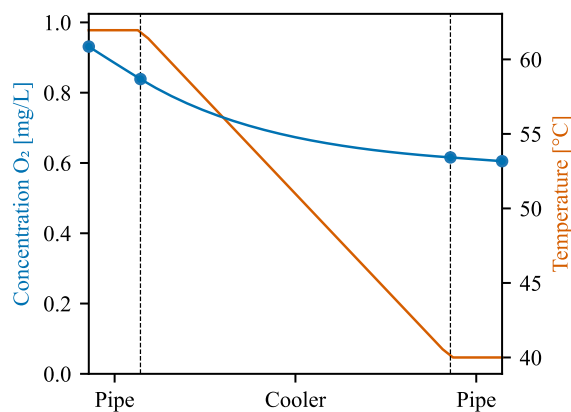**Fig. 31.** Process flow diagram of in-and-out intercooling in the absorber.

Table 7
Predicted degradation in the absorber and intercooling loop for the reference case for the coal–fired power plant flue gas, the ideal intercooled case with no additional holdup, and the realistic intercooled case with the intercooling loop and additional distribution.

Degradation [g MEA/ton CO_2]	Reference case	Intercooled (in-situ)	Intercooled (in-and-out)
Absorber	59.9	36.7	39.5
→ Structured packing	45.3	23.8	23.8
→ Collectors/distributors	4.6	3.1	5.8
→ Sump	10.0	9.9	9.9
Intercooling loop	–	–	6.6
Total (process)	89.1	66.8	76.1

absorber sump effectively reduces degradation rates in the stripper and heat exchanger as is shown in Fig. 26. Degradation in the other parts of the process is unchanged. The predicted overall degradation for this case study is 74.1 g MEA/ton CO_2, which is a reduction of 16.8%.

The overall impact of dissolved O_2 removal is limited for MEA since a large fraction of oxidative degradation occurs in the absorber. Solvents that are more stable towards oxidative degradation at typical absorber temperatures are still expected to degrade oxidatively as the temperature increases in the heat exchanger. Degradation as a result of dissolved O_2 is expected to play a larger role for these solvents, and dissolved O_2 removal can have a larger impact.

It is important to study oxidative degradation at heat exchanger conditions for these solvents, as the reaction order of O_2 can play an important role. For example, if the dependency of the reaction rate on the concentration of O_2 is relatively low, the degradation rate will not change by removing dissolved O_2. The impact of dissolved O_2 removal may then be limited in cases where the amount of O_2 left behind is larger than the amount of O_2 consumed by degradation.

3.4.2. Change in capture efficiency

Increasing the capture rate to 95%, increases the degradation rate per ton of CO_2 in the absorber packing and distributors by 57.7%, due to the additional packing height and the added collector and distributor (Fig. 26). The solvent flow rate was increased by 5.6%, which causes the degradation in the other parts of the process to increase slightly. However, since more CO_2 is captured in this case study, the degradation rate relative to the amount of CO_2 captured is unchanged. Since most of the degradation is caused by direct oxidative degradation in the packing, mitigation strategies that aim at reducing thermal degradation or indirect oxidative degradation through dissolved O_2 will be less effective at increased capture efficiencies.

A capture process with a reduced capture efficiency of 85% was also

investigated. Apart from a marginal reduction in degradation in the absorber packing and distributors (-20.9%), similar degradation is expected in the other parts of the process. However, as the degradation rates are normalized to the CO_2 captured, the absolute degradation in the process would be lower.

3.4.3. Stripper pressure

The predicted degradation for the case study with a stripper pressure of 2.5 bar is shown in Fig. 26. Thermal degradation in this case study is increased by 200% with respect to the reference case, because at this pressure, the temperatures in the stripper are higher, especially in the sump and reboiler. Aside from a slight increase in thermal degradation in the heat exchanger, degradation in the rest of the simulated process is the same. The overall degradation rate is predicted to be 133.2 g MEA/ton CO_2.

Léonard et al. (Léonard et al., 2015) also investigated the effect of increased stripper pressures on the total degradation but observed a significantly smaller increase. However, the contribution of thermal degradation was negligible in the predictions by Léonard et al. (Léonard et al., 2015), so although an increase in thermal degradation was observed, the total degradation was not influenced significantly.

The thermal and total degradation rate as a function of the stripper pressure is shown in Fig. 33. At a constant solvent flow rate, the energy duty in the reboiler that is required to capture 90% CO_2 in the process decreases as the stripper pressure increases. At a stripper pressure of 3.0 bar, the temperature in the stripper reboiler is 134 °C. At this point, the total predicted degradation is 188.7 g MEA/ton CO_2, which is more than double the degradation in the reference case. More than half of the degradation at a stripper pressure of 3.0 bar is due to thermal degradation in the stripper.

A good operating strategy would thus select a stripper pressure that benefits from the reduced energy requirements, without the occurrence of significant thermal degradation. However, as degradation causes other operational problems, potentially increased emission mitigation requirements, and increased costs, optimizing the reboiler pressure is in reality a complex design problem.

3.4.4. Reduced solvent residence times

A 50% reduction in solvent residence time of the equipment, as specified in Table 4, reduces degradation by 13.7%, for a total of 76.9 g MEA/ton CO_2. Degradation in the packing is reduced only slightly and this shows that only a small fraction of degradation is occurring in the collectors and distributors. Most of the degradation is taking place in the packing itself, where the residence time is not changed.

Even though degradation in the absorber sump is reduced, the unreacted dissolved O_2 is now consumed in the heat exchanger. The residence time in this equipment is also reduced, but the low stability of

MEA at increased temperatures causes all of the O_2 to still be consumed. A reduction in residence times may be more effective for solvents that are more stable toward oxidative degradation. In those solvents, complete depletion of O_2 in the heat exchanger may not occur and exposure time is more important.

Degradation in the stripper sump and reboiler is halved. Since this thermal degradation only makes up a limited percentage of the total degradation, the effects here are limited. However, in cases where thermal degradation is more prominent, a reduction of residence time could be valuable. This could be the case for solvents that are more resistant toward oxidative degradation, for processes with flue gases with a low O_2 content, or in case the stripper pressure is increased. Residence times in the stripper may be reduced for example by combining the sump and reboiler. Finally, degradation in the pumps and cooler is limited and the effect of reduced residence times on the overall degradation is negligible.

3.4.5. Oxygen concentration in the flue gas

Fig. 34 shows that oxidative degradation is expected to be the dominant degradation mechanism for post-combustion capture processes. Thermal degradation is predicted to be dominant, only in case the flue gas contains less than 1 vol% of O_2. The extent of indirect oxidative degradation appears to be linearly proportional to the concentration of O_2 in the flue gas. This is caused by the linear dependency of the solubility of O_2 on the partial pressure of O_2 at absorber conditions and the fact that all of the dissolved O_2 will react. This means that a change in the solubility of O_2 will have a similar effect on degradation as a change in O_2 partial pressure.

The distribution of the degradation in the various parts of the process is shown in Fig. 35 and Fig. 36. Higher O_2 concentrations in the flue gas lead to an increase in direct oxidative degradation in the absorber packing. The increase is more prominent at lower O_2 concentrations, which is a result of the reaction order for O_2 in the rate equation (n = 0.47). An increase in degradation is observed in the heat exchanger at higher O_2 concentrations since more dissolved O_2 remains in the rich solvent exiting the absorber sump. There is no oxidative degradation in the stripper and thermal degradation in equipment other than the stripper is limited. Therefore, the extent of degradation in the stripper remains unchanged. Degradation in other parts of the process is limited.

3.4.6. Reduced oxidative degradation rate

The effects of a reduction in oxidative degradation rate on the overall oxidative and thermal degradation and degradation in various parts of the process are shown in Fig. 37 and Fig. 38, respectively. Degradation in the absorber packing is linearly proportional to the degradation rate coefficient. A small reduction in the oxidative degradation rate has no
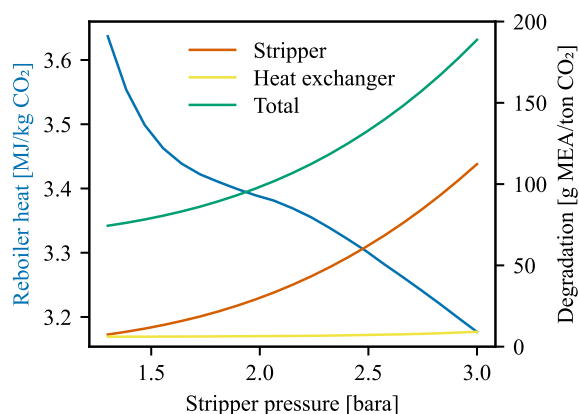

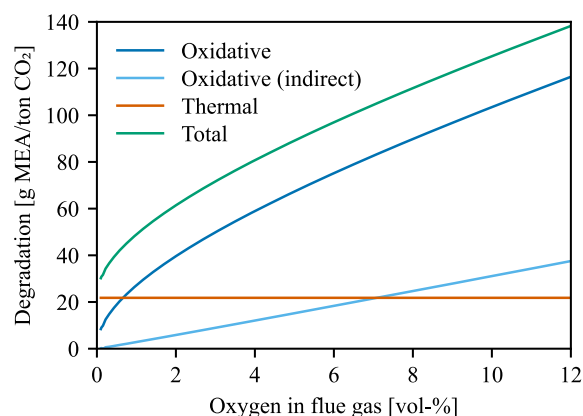**Fig. 33.** Impact of stripper pressure on required reboiler heat and solvent degradation.

Fig. 34. Predicted oxidative and thermal degradation in the reference case as a function of the concentration of O_2 in the flue gas, also showing the contribution of indirect oxidative degradation through dissolved O_2.
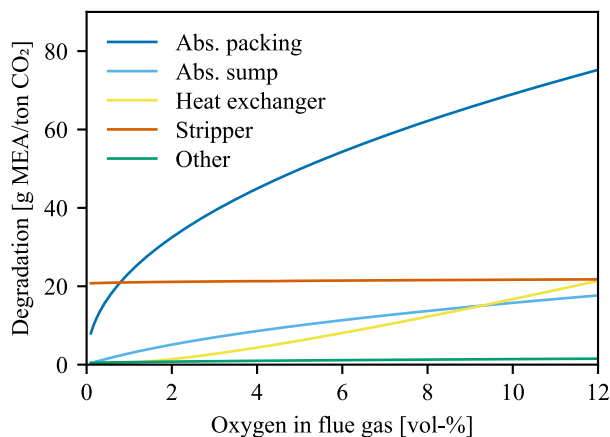
Fig. 35. Predicted degradation for equipment in the reference case as a function of the concentration of O_2 in the flue gas.
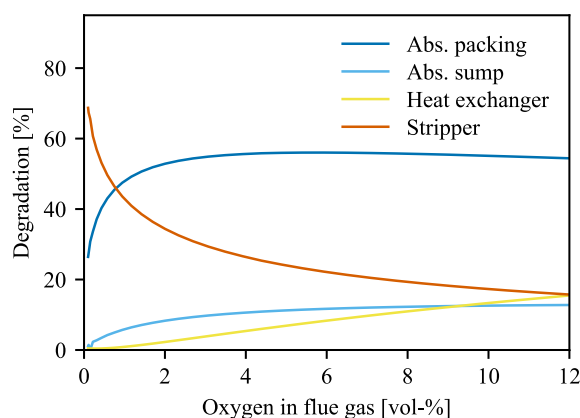

Fig. 36. Predicted distribution of degradation for equipment in the reference case as a function of the concentration of O_2 in the flue gas.

impact on the amount of degradation through dissolved O_2. Oxidative degradation in the sump is reduced, but the remaining O_2 is now consumed in the heat exchanger.

At around 30% of the initial degradation rate, full consumption of O_2 in the heat exchanger no longer occurs and the remaining dissolved O_2 is consumed in the sequential pipe leading up to the stripper inlet. Degradation in this pipe is responsible for the majority of the degradation labeled as "Other" in Fig. 38.
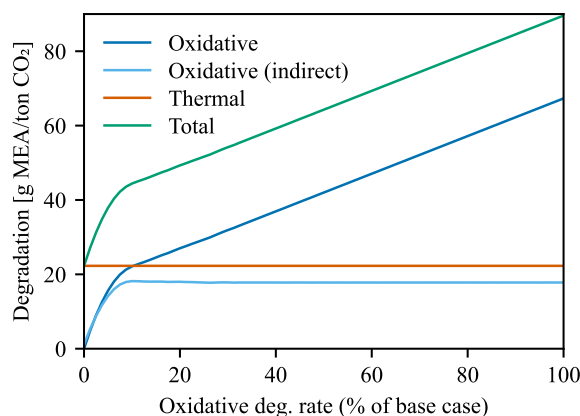

Fig. 37. Predicted oxidative and thermal degradation in the reference case as a function of the oxidative degradation rate, also showing the contribution of indirect oxidative degradation through dissolved O_2.
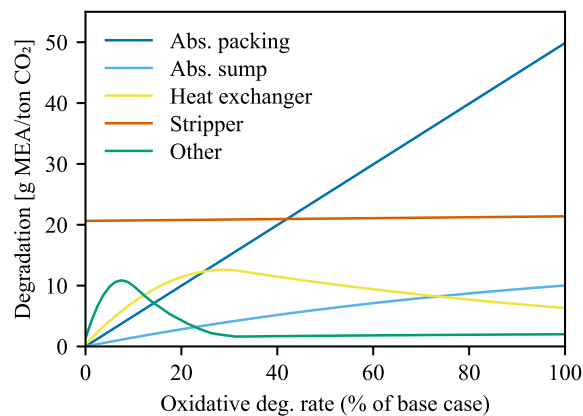

Fig. 38. Predicted degradation for equipment in the reference case as a function of the oxidative degradation rate. By far the largest contribution to Other is degradation in the pipe from the heat exchanger to the stripper.

When the oxidative degradation is reduced to 10% of the initial rate, there is a breakthrough of dissolved O_2 into the stripper. This behavior is illustrated in Fig. 39, where all of the initially dissolved O_2 is just consumed. A significant part of the dissolved O_2 is consumed in the pipe leading up to the stripper, even though the residence time in this pipe is only 20 s. A higher liquid velocity in this pipe, leading to a lower residence time may be an effective way of reducing degradation in such a case.

The more stable a solvent is towards oxidative degradation, the larger the relative contributions of degradation by dissolved O_2 and thermal degradation will be. Mitigation strategies that aim at reducing these types of degradation, such as a reduction in residence times or stripper pressure, or removal of dissolved O_2, will thus be more effective for these stable solvents.

4. Conclusion

This work focused on solvent degradation in absorption-based CO_2 capture processes using a 30 wt% aqueous monoethanolamine (MEA) solvent. A degradation model for MEA was developed and used to predict solvent degradation in full-scale capture processes. Degradation in the base case capture processes for the investigated flue gases was predicted to be 90 to 150 g MEA/ton CO_2, which is lower than typically observed in pilot plants. In these plants, however, iron and other metals are expected to dissolve and catalyze the degradation. The degradation model in this work does not take this accelerated degradation into account and this is the most likely cause of the underprediction. Additional experimental data is required to accurately model the catalyzed reactions and the rate equations that describe corrosion and dissolved
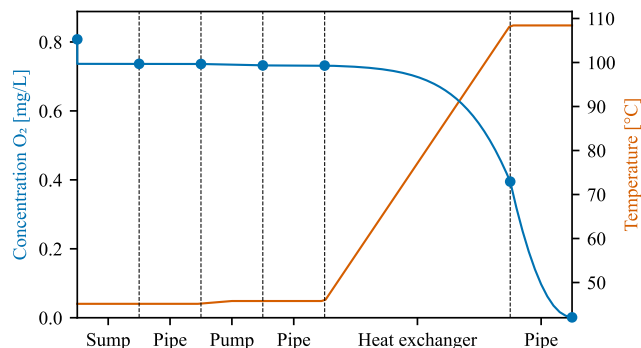

Fig. 39. Liquid temperature and predicted concentration of dissolved O_2 in the rich solvent from the absorber sump to the inlet of the stripper at an oxidative degradation rate of 10% the rate of the reference case.

metal concentrations, which should then be included in future iterations of degradation models.

The high CO_2 content of the flue gas for the coal and cement cases leads to increased temperatures in the absorber and relatively high degradation rates. The natural gas and WTE cases, on the other hand, are characterized by more indirect oxidative degradation, due to the relatively high concentration of O_2 in the flue gas and rich solvent. The degree of thermal degradation is similar for all the cases, accounting for approximately 10% to 20% of the total degradation.

Modifications to the base case capture process for a coal–fired power plant can have a significant effect on the degradation. A reduction of temperatures in the absorber packing can reduce degradation up to 84.6% if an isothermal absorber would be implemented. A single in-situ intercooling stage at the peak of the temperature bulge reduces the total degradation in the process by 25.0%. However, the additional solvent holdup and exposure as a result of implementing the intercooling may negate some of these benefits. An in-and-out intercooler placed at ground level generates additional degradation and is estimated to only lead to a 14.6% net reduction in the overall degradation.

Dissolved O_2 removal can be effective at reducing indirect oxidative degradation. However, due to the relatively small contribution of this type of degradation to the total degradation in the coal–fired flue gas case, the overall impact is limited for 30 wt% MEA. The extent of indirect oxidative degradation will be more significant in processes with higher concentrations of O_2 in the flue gas or for solvents that are more stable towards oxidative degradation at absorber temperatures. Timely removal of the dissolved O_2 may play an important role here. An increase in stripper pressure is found to both decrease heat requirements and increase degradation significantly. More information about the impact of degradation and the degradation products on, for example, the performance of the process or the costs of reclaiming is required to select the optimal operating point.

The impact of reduced residence times in the column sumps and reboilers, heat exchanger, pumps, and piping is limited for the process with MEA as a solvent. Despite a smaller exposure time for the rich solvent on its way to the stripper, all of the dissolved O_2 is still consumed. The effect will be more significant in case the stability of the solvent is higher and some of the dissolved O_2 does not react. For similar reasons, an increase in solvent stability or a reduction in the oxidative degradation rate has initially little effect on the extent of indirect oxidative degradation. Only the direct oxidative degradation in the absorber packing is reduced. At an oxidative degradation rate that is lower than 17.5% the rate for MEA, a fraction of the dissolved O_2 is not consumed and enters the stripper. This results in less indirect oxidative degradation and a larger reduction in the overall degradation.

The liquid phase mass transfer limitations of O_2 in the absorber packing have been estimated and are found to be negligible, so the solvent is saturated with O_2 in the packing. This is, however, not always the case for oxidative degradation experiments. Experiments in an agitated bubble reactor are likely to involve significant liquid phase mass transfer resistances, especially at the higher temperatures that are typical for the absorber. In this work, these resistances have been considered and a rate equation for the consumption of MEA has been fitted using the experimental data by Vevelstad et al. (Vevelstad et al., 2016). The deviations of the oxidative degradation model were significant, but no clear trends were observed in the residuals. The experimental uncertainty is expected to play an important role in the uncertainty of the model but could not be quantified accurately.

To develop more accurate oxidative degradation models, the degradation kinetics should be separated from mass transfer resistances. Correlations used to estimate mass transfer resistances can be uncertain because they rely on a generalization of mass transfer processes. In addition, the quantification of the process parameters, such as the bubble diameter or stirring power, can be challenging. Oxidative degradation reactors should therefore be designed to eliminate mass transfer resistances so that the observed degradation is directly related to the reaction kinetics. This can be achieved by for example increasing the interfacial area or reducing the liquid volume fraction in the reactor. Alternatively, if the elimination of mass transfer resistances is not feasible, the degradation reactor should be designed such that these can be quantified accurately.

The solubility of O_2 and its temperature dependency are important parameters to evaluate oxidative degradation since the concentration of dissolved O_2 can be directly proportional to the extent of degradation in the absorber sump, cross-heat exchanger, and related piping. Therefore, accurate quantification of this solubility is valuable. But this may be hard to achieve because of consumption by the degradation reactions. Alternatively, solubility models can be used to develop degradation models, but these degradation models should not be used independently or combined with other solubility models, and the impact of the CO_2 loading on the solubility of O_2 should be considered.

Declaration of Competing Interest

The authors declare that they have no known competing financial interests or personal relationships that could have appeared to influence the work reported in this paper.

Data availability

No data was used for the research described in the article.

References

Abu-Zahra, M.R.M., Schneiders, L.H.J., Niederer, J.P.M., Feron, P.H.M., Versteeg, G.F., 2007. CO2 Capture from Power Plants: Part I. A Parametric Study of the Technical Performance Based on Monoethanolamine. Int. J. Greenhouse Gas Control 1 (1), 37–46. https://doi.org/10.1016/S1750-5836(06)00007-7.

Amrollahi, Z., Ystad, P.A.M., Ertesvåg, I.S., Bolland, O., 2012. Optimized Process Configurations of Post-Combustion CO2 Capture for Natural-Gas-Fired Power Plant – Power Plant Efficiency Analysis. Int. J. Greenhouse Gas Control 8, 1–11. https://doi.org/10.1016/j.ijggc.2012.01.005.

Arnaut, L. Chapter 4 - Reaction Order and Rate Constants. In *Chemical Kinetics (Second Edition)*; Arnaut, L., Ed.; Elsevier, 2021; pp 93–138. https://doi.org/10.1016/B978-0-444-64039-0.00014-5.

Aronu, U. E.; Ghondal, S.; Hessen, E. T.; Haug-Warberg, T.; Hoff, K. A.; Svendsen, H. F. Equilibrium in the H2O-MEA-CO2 System: New Data and Modeling. 3. Conference proceedings at PCCC-1 (Post Combustion Capture Conference), 2011.

Bello, A., Idem, R.O., 2006. Comprehensive Study of the Kinetics of the Oxidative Degradation of CO2 Loaded and Concentrated Aqueous Monoethanolamine (MEA) with and without Sodium Metavanadate during CO2 Absorption from Flue Gases. Ind. Eng. Chem. Res. 45 (8), 2569–2579. https://doi.org/10.1021/ie050562x.

Benson, B.B., Krause, D., Peterson, M.A., 1979. The Solubility and Isotopic Fractionation of Gases in Dilute Aqueous Solution. I. Oxygen. *J Solution Chem* 8 (9), 655–690. https://doi.org/10.1007/BF01033696.

Billet, R., Schultes, M., 1999. Prediction of Mass Transfer Columns with Dumped and Arranged Packings: Updated Summary of the Calculation Method of Billet and Schultes. Chem. Eng. Res. Des. 77 (6), 498–504. https://doi.org/10.1205/026387699526520.

Braakhuis, L.; Knuutila, H. K. Modelling and Evaluating Carbamate Polymerization of Monoethanolamine in Post-Combustion Carbon Capture. In *SINTEF Proceedings*; Trondheim, 2021.

Buvik, V., Høisæter, K.K., Vevelstad, S.J., Knuutila, H.K., 2021. A Review of Degradation and Emissions in Post-Combustion CO2 Capture Pilot Plants. Int. J. Greenhouse Gas Control 106, 103246. https://doi.org/10.1016/j.ijggc.2020.103246.

Buvik, V., Bernhardsen, I.M., Figueiredo, R.V., Vevelstad, S.J., Goetheer, E., van Os, P., Knuutila, H.K., 2021. Measurement and Prediction of Oxygen Solubility in Post-Combustion CO2 Capture Solvents. Int. J. Greenhouse Gas Control 104, 103205. https://doi.org/10.1016/j.ijggc.2020.103205.

Chi, S., 2000. Oxidative Degradation of Monoethanolamine. University of Kentucky.

Cussler, E.L., Cussler, E.L., 2009. Diffusion: Mass Transfer in Fluid Systems. Cambridge University Press.

Davis, J.D., 2009. Thermal Degradation of Aqueous Amines Used for Carbon Dioxide Capture. The University of Texas, Austin https://repositories.lib.utexas.edu/handle/2152/6581.

Dhingra, S., Khakharia, P., Rieder, A., Cousins, A., Reynolds, A., Knudsen, J., Andersen, J., Irons, R., Mertens, J., Abu Zahra, M., Van Os, P., Goetheer, E., 2017. Understanding and Modelling the Effect of Dissolved Metals on Solvent Degradation in Post Combustion CO2 Capture Based on Pilot Plant Experience. Energies 10 (5), 629. https://doi.org/10.3390/en10050629.

Eide-Haugmo, I., 2011. Environmental Impacts and Aspects of Absorbents Used for CO2 Capture. Norwegian University of Science and Technology, Trondheim.

GPSA Engineering Data Book, 12th ed.; Gas Processors Suppliers Association, 2004.

Fagerlund, J., Zevenhoven, R., Thomassen, J., Tednes, M., Abdollahi, F., Thomas, L., Nielsen, C.J., Mikoviny, T., Wisthaler, A., Zhu, L., Biliyok, C., Zhurkin, A., 2021. Performance of an Amine-Based CO2 Capture Pilot Plant at the Fortum Oslo Varme Waste to Energy Plant in Oslo, Norway. Int. J. Greenhouse Gas Control 106, 103242. https://doi.org/10.1016/j.ijggc.2020.103242.

Fredriksen, S.B., Jens, K.-J., 2013. Oxidative Degradation of Aqueous Amine Solutions of MEA, AMP, MDEA, Pz: A Review. Energy Procedia 37, 1770–1777.

Freguia, S., Rochelle, G.T., 2003. Modeling of CO2 Capture by Aqueous Monoethanolamine. AIChE J 49 (7), 1676–1686. https://doi.org/10.1002/aic.690490708.

Geankoplis, C.J., Hersel, A.A., Lepek, D.H., 2018. Transport Processes and Separation Process Principles. Prentice Hall.

Goff, G.S., Rochelle, G.T., 2004. Monoethanolamine Degradation: O₂ Mass Transfer Effects under CO₂ Capture Conditions. Ind. Eng. Chem. Res. 43 (20), 6400–6408. https://doi.org/10.1021/ie0400245.

Goff, G. S. Oxidative Degradation of Aqueous Monoethanolamine in CO2 Capture Processes: Iron and Copper Catalysis, Inhibition, and O2 Mass Transfer. **2005**, 283.

Gouedard, C., Picq, D., Launay, F., Carrette, P.-L., 2012. Amine Degradation in CO2 Capture. I. A Review. Int. J. Greenhouse Gas Control 10, 244–270. https://doi.org/10.1016/j.ijggc.2012.06.015.

Grimstvedt, A.; Falck da Silva, E.; Hoff, K. A. Thermal Degradation of MEA, Effect of Temperature and CO2 Loading; SINTEF Materials and Chemistry, Trondheim, TCCS-7, 2013.

Herraiz, L., Fernández, E.S., Palfi, E., Lucquiaud, M., 2018. Selective Exhaust Gas Recirculation in Combined Cycle Gas Turbine Power Plants with Post-Combustion CO2 Capture. Int. J. Greenhouse Gas Control 71, 303–321. https://doi.org/10.1016/j.ijggc.2018.01.017.

Jakobsen, J.P., Krane, J., Svendsen, H.F., 2005. Liquid-Phase Composition Determination in CO2−H2O−Alkanolamine Systems: An NMR Study. Ind. Eng. Chem. Res. 44 (26), 9894–9903. https://doi.org/10.1021/ie048813+.

Kasikamphaiboon, P., Chungsiriporn, J., Bunyakan, C., Wiyaratn, W., 2015. Degradation Kinetics of Monoethanolamine during CO2 and H2S Absorption from. Biogas. 9.

Knudsen, J.N., Jensen, J.N., Vilhelmsen, P.-J., Biede, O., 2009. Experience with CO2 Capture from Coal Flue Gas in Pilot-Scale: Testing of Different Amine Solvents. Energy Procedia 1 (1), 783–790. https://doi.org/10.1016/j.egypro.2009.01.104.

Knudsen, J.N., Andersen, J., Jensen, J.N., Biede, O., 2011. Evaluation of Process Upgrades and Novel Solvents for the Post Combustion CO2 Capture Process in Pilot-Scale. Energy Procedia 4, 1558–1565. https://doi.org/10.1016/j.egypro.2011.02.025.

Knudsen, J.N., Bade, O.M., Askestad, I., Gorset, O., Mejdell, T., 2014. Pilot Plant Demonstration of CO2 Capture from Cement Plant with Advanced Amine Technology. Energy Procedia 63, 6464–6475. https://doi.org/10.1016/j.egypro.2014.11.682.

Kohl, A.L., Nielsen, R.B., 1997. Alkanolamines for Hydrogen Sulfide and Carbon Dioxide Removal. In: Gas Purification. Elsevier, pp. 40–186. https://doi.org/10.1016/B978-088415220-0/50002-1.

Kvamsdal, H.M., Rochelle, G.T., 2008. Effects of the Temperature Bulge in CO2 Absorption from Flue Gas by Aqueous Monoethanolamine. Ind. Eng. Chem. Res. 47 (3), 867–875. https://doi.org/10.1021/ie061651s.

Léonard, G., 2013. Optimal Design of a CO2 Capture Unit with Assessment of Solvent Degradation. Université de Liège.

Léonard, G., Voice, A., Toye, D., Heyen, G., 2014. Influence of Dissolved Metals and Oxidative Degradation Inhibitors on the Oxidative and Thermal Degradation of Monoethanolamine in Postcombustion CO₂ Capture. Ind. Eng. Chem. Res. 53 (47), 18121–18129. https://doi.org/10.1021/ie5036572.

Léonard, G., Toye, D., Heyen, G., 2014. Experimental Study and Kinetic Model of Monoethanolamine Oxidative and Thermal Degradation for Post-Combustion CO₂ Capture. Int. J. Greenhouse Gas Control 30, 171–178. https://doi.org/10.1016/j.ijggc.2014.09.014.

Léonard, G., Toye, D., Heyen, G., 2014. Assessment of Solvent Degradation within a Global Process Model of Post-Combustion CO2 Capture. In: Computer Aid. Chem. Eng., Vol. 33. Elsevier, pp. 13–18. https://doi.org/10.1016/B978-0-444-63456-6.50003-X.

Léonard, G., Crosset, C., Toye, D., Heyen, G., 2015. Influence of Process Operating Conditions on Solvent Thermal and Oxidative Degradation in Post-Combustion CO2 Capture. Comput. Chem. Eng. 83, 121–130. https://doi.org/10.1016/j.compchemeng.2015.05.003.

Lepaumier, H., Picq, D., Carrette, P.-L., 2009. New Amines for CO₂ Capture. II. Oxidative Degradation Mechanisms. Ind. Eng. Chem. Res. 48 (20), 9068–9075. https://doi.org/10.1021/ie9004749.

Lepaumier, H., da Silva, E.F., Einbu, A., Grimstvedt, A., Knudsen, J.N., Zahlsen, K., Svendsen, H.F., 2011. Comparison of MEA Degradation in Pilot-Scale with Lab-Scale Experiments. Energy Procedia 4, 1652–1659. https://doi.org/10.1016/j.egypro.2011.02.037.

Magnanelli, E., Mosby, J., Becidan, M., 2021. Scenarios for Carbon Capture Integration in a Waste-to-Energy Plant. Energy 227, 120407. https://doi.org/10.1016/j.energy.2021.120407.

Martin, S., Lepaumier, H., Picq, D., Kittel, J., de Bruin, T., Faraj, A., Carrette, P.-L., 2012. New Amines for CO2 Capture. IV. Degradation, Corrosion, and Quantitative Structure Property Relationship Model. Ind. Eng. Chem. Res. 51 (18), 6283–6289. https://doi.org/10.1021/ie2029877.

Moser, P.; Wiechers, G.; Schmidt, S.; Garcia Moretz-Sohn Monteiro, J.; Charalambous, C.; Garcia, S.; Sanchez Fernandez, E. Results of the 18-Month Test with MEA at the Post-Combustion Capture Pilot Plant at Niederaussem – New Impetus to Solvent Management, Emissions and Dynamic Behaviour. *Int. J. Greenhouse Gas Control* **2020**, *95*, 102945. https://doi.org/10.1016/j.ijggc.2019.102945.

Nielsen, P. Oxidation of Piperazine in Post-Combustion Carbon Capture, The University of Texas, 2018. https://repositories.lib.utexas.edu/bitstream/handle/2152/68015/NIELSEN-DISSERTATION-2018.pdf.

Pinto, D.D.D., Brodtkorb, T.W., Vevelstad, S.J., Knuutila, H., Svendsen, H.F., 2014. Modeling of Oxidative MEA Degradation. Energy Procedia 63, 940–950. https://doi.org/10.1016/j.egypro.2014.11.103.

Puxty, G.; Maeder, M. 2 - The Fundamentals of Post-Combustion Capture. In *Absorption-Based Post-combustion Capture of Carbon Dioxide*; Feron, P. H. M., Ed.; Woodhead Publishing, 2016; pp 13–33. Doi: 10.1016/B978-0-08-100514-9.00002-0.

Rao, A.B., Rubin, E.S., 2002. A Technical, Economic, and Environmental Assessment of Amine-Based CO2 Capture Technology for Power Plant Greenhouse Gas Control. Environ. Sci. Tech. 36 (20), 4467–4475. https://doi.org/10.1021/es0158861.

Reynolds, A.J., Verheyen, T.V., Meuleman, E., 2016. Degradation of Amine-Based Solvents. In: Absorption-Based Post-combustion Capture of Carbon Dioxide. Elsevier, pp. 399–423. https://doi.org/10.1016/B978-0-08-100514-9.00016-0.

Rogelj, J., Shindell, D., Jiang, K., Fifita, S., Forster, P., Ginzburg, V., 2018. Mitigation Pathways Compatible with 1.5°C in the Context of Sustainable Development; Intergovernmental Panel on. Clim. Change.

Rooney, P.C., Daniels, D.D., 1998. Oxygen Solubility in Various Alkanolamine/Water Mixtures. Pet. Technol. Q. 97–101.

Rooney, P.C., Dupart, M.S., Bacon, T.R., 1998. Oxygen's Role in Alkanolamine Degradation. Hydrocarb. Process. 77, 109–113.

Sexton, A.J., 2008. Amine Oxidation in CO2 Capture Processes. The University of Texas.

Staab, G.; Fine, N.; Panaccione, C.; Atcheson, J.; Silverman, T.; Brown, A. E.; Meuleman, E. Modular Adaptive Packing for Integrally Cooled Absorbers. Rochester, NY November 28, 2022. https://doi.org/10.2139/ssrn.4288015.

Strigle, R.F., 1987. Packed Tower Design and Applications. Gulf Publishing Co, U.S.

Supap, T., Idem, R., Veawab, A., Aroonwilas, A., Tontiwachwuthikul, P., Chakma, A., Kybett, B.D., 2001. Kinetics of the Oxidative Degradation of Aqueous Monoethanolamine in a Flue Gas Treating Unit. Ind. Eng. Chem. Res. 40 (16), 3445–3450. https://doi.org/10.1021/ie000957a.

Supap, T., Idem, R., Tontiwachwuthikul, P., Saiwan, C., 2009. Kinetics of Sulfur Dioxide- and Oxygen-Induced Degradation of Aqueous Monoethanolamine Solution during CO2 Absorption from Power Plant Flue Gas Streams. Int. J. Greenhouse Gas Control 3 (2), 133–142. https://doi.org/10.1016/j.ijggc.2008.06.009.

Tobiesen, F.A., Svendsen, H.F., Juliussen, O., 2007. Experimental Validation of a Rigorous Absorber Model for CO2 Postcombustion Capture. AIChE J 53 (4), 846–865. https://doi.org/10.1002/aic.11133.

Tobiesen, F.A., Juliussen, O., Svendsen, H.F., 2008. Experimental Validation of a Rigorous Desorber Model for CO2 Post-combustion Capture. Chem. Eng. Sci. 63 (10), 2641–2656. https://doi.org/10.1016/j.ces.2008.02.011.

Towler, G.; Sinnott, R. Chapter 19 - Heat-Transfer Equipment. In *Chemical Engineering Design (Second Edition)*; Towler, G., Sinnott, R., Eds.; Butterworth-Heinemann: Boston, 2013; pp 1047–1205. Doi: 10.1016/B978-0-08-096659-5.00019-5.

Uyanga, I.J., Idem, R.O., 2007. Studies of SO2- and O2-Induced Degradation of Aqueous MEA during CO2 Capture from Power Plant Flue Gas Streams. Ind. Eng. Chem. Res. 46 (8), 2558–2566. https://doi.org/10.1021/ie0614024.

V. Figueiredo, R.; Srivastava, T.; Skaar, T.; Warning, N.; Gravesteijn, P.; van Os, P.; Ansaloni, L.; Deng, L.; Knuutila, H.; Monteiro, J.; Goetheer, E. Impact of Dissolved Oxygen Removal on Solvent Degradation for Post-Combustion CO2 Capturew. *Int. J. Greenhouse Gas Control* **2021**, *112*, 103493. Doi: 10.1016/j.ijggc.2021.103493.

Vega, F., Sanna, A., Navarrete, B., Maroto-Valer, M.M., Cortés, V.J., 2014. Degradation of Amine-Based Solvents in CO2 Capture Process by Chemical Absorption. Greenhouse Gases Sci. Technol. 4 (6), 707–733. https://doi.org/10.1002/ghg.1446.

Veltman, K., Singh, B., Hertwich, E.G., 2010. Human and Environmental Impact Assessment of Postcombustion CO2 Capture Focusing on Emissions from Amine-Based Scrubbing Solvents to Air. Environ. Sci. Tech. 44 (4), 1496–1502. https://doi.org/10.1021/es902116r.

Vevelstad, S.J., Johansen, M.T., Knuutila, H., Svendsen, H.F., 2016. Extensive Dataset for Oxidative Degradation of Ethanolamine at 55–75°C and Oxygen Concentrations from 6 to 98%. Int. J. Greenhouse Gas Control 50, 158–178. https://doi.org/10.1016/j.ijggc.2016.04.013.

Vevelstad, S.J., Grimstvedt, A., Haugen, G., Kupfer, R., Brown, N., Einbu, A., Vernstad, K., Zahlsen, K., 2017. Comparison of Different Solvents from the Solvent Degradation Rig with Real Samples. Energy Procedia 114, 2061–2077. https://doi.org/10.1016/j.egypro.2017.03.1341.

Voice, A.K., Closmann, F., Rochelle, G.T., 2013. Oxidative Degradation of Amines With High-Temperature Cycling. Energy Procedia 37, 2118–2132. https://doi.org/10.1016/j.egypro.2013.06.091.

Wang, M.H., Ledoux, A., Estel, L., 2013. Oxygen Solubility Measurements in a MEA/H2O/CO2 Mixture. J. Chem. Eng. Data 58 (5), 1117–1121. https://doi.org/10.1021/je301077y.

Warudkar, S.S., Cox, K.R., Wong, M.S., Hirasaki, G.J., 2013. Influence of Stripper Operating Parameters on the Performance of Amine Absorption Systems for Post-Combustion Carbon Capture: Part I. High Pressure Strippers. Int. J. Greenhouse Gas Control 16, 342–350. https://doi.org/10.1016/j.ijggc.2013.01.050.

Weiland, R.H., Dingman, J.C., Cronin, D.B., Browning, G.J., 1998. Density and Viscosity of Some Partially Carbonated Aqueous Alkanolamine Solutions and Their Blends. J. Chem. Eng. Data 43 (3), 378–382. https://doi.org/10.1021/je9702044.

Weisenberger, S., Schumpe, A., 1996. Estimation of Gas Solubilities in Salt Solutions at Temperatures from 273 K to 363 K. AIChE J 42 (1), 298–300. https://doi.org/10.1002/aic.690420130.

Wu, Y., 2022. Mitigation Methods for Piperazine Oxidation in Post-Combustion Carbon Capture. Thesis. https://doi.org/10.26153/tsw/43500.

Zhang, Y., Chen, H., Chen, C.-C., Plaza, J.M., Dugas, R., Rochelle, G.T., 2009. Rate-Based Process Modeling Study of CO2 Capture with Aqueous Monoethanolamine Solution. Ind. Eng. Chem. Res. 48 (20), 9233–9246. https://doi.org/10.1021/ie900068k.